iScience

CellPress
OPEN ACCESS

Article

Quiescence and aging of melanocyte stem cells and a novel association with programmed death-ligand 1

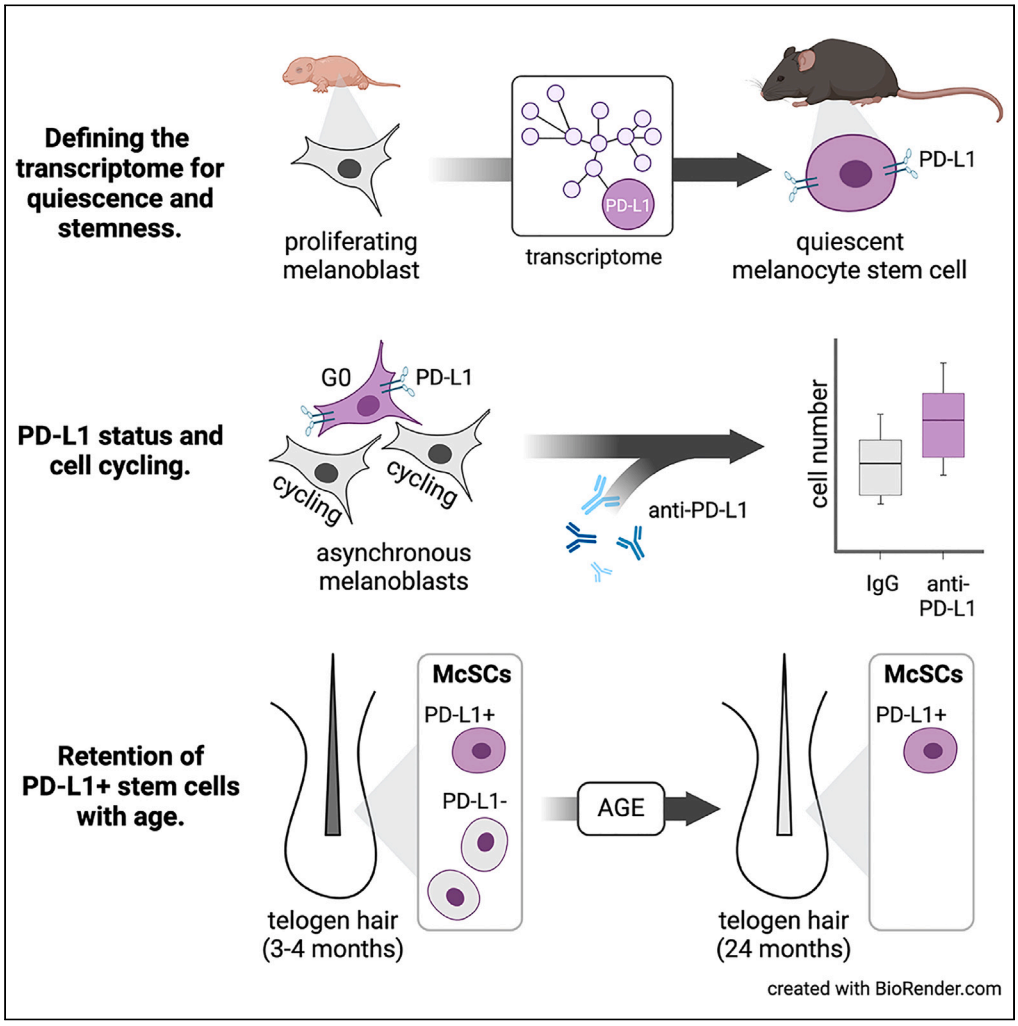

Joseph W. Palmer, Kyrene M. Villavicencio, Misgana Idris, ..., William J. Pavan, Fabian V. Filipp, Melissa L. Harris

harrisml@uab.edu

Highlights

Melanocyte stem cells (McSCs) actively maintain quiescence

Aged McSCs show an enhanced quiescent but not senescent transcriptome

PD-L1 marks some quiescent McSCs and inhibits proliferation in cell models

PD-L1+ McSCs that persist with age may be good targets for reactivation

Palmer et al., iScience 27, 110908
October 18, 2024
https://doi.org/10.1016/j.isci.2024.110908

iScience

CellPress
OPEN ACCESS

Article

Quiescence and aging of melanocyte stem cells and a novel association with programmed death-ligand 1

Joseph W. Palmer,[1] Kyrene M. Villavicencio,[1] Misgana Idris,[1] Ian J. Baranyk,[1] Nunaya Polycarp,[1] Alex D. Dawson,[1] Dominique Weddle,[1] NISC Comparative Sequencing Program,[2] William J. Pavan,[3] Fabian V. Filipp,[4,5,6,7] and Melissa L. Harris[1,8,*]

SUMMARY

Cellular quiescence is a reversible and tightly regulated stem cell function essential for healthy aging. However, the elements that control quiescence during aging remain poorly defined. Using melanocyte stem cells (McSCs), we find that stem cell quiescence is neither passive nor static. For example, gene expression profiling of the transition from proliferating melanoblasts to quiescent melanocyte stem cells reveals tissue-specific regulation of the immune checkpoint protein PD-L1. *In vitro*, quiescence assays demonstrate that PD-L1 expression is a physiological attribute of quiescence in this cell lineage and reinforces this cell state. *In vivo*, a subset of quiescent McSCs is marked by PD-L1. While the overall number of McSCs decreases with age, PD-L1+ McSCs appear resistant to depletion. This phenomenon coincides with an aged McSC pool that exhibits a deeper transcriptomic quiescence. We predict that quiescent PD-L1+ stem cells retained with age may serve as cellular targets for reactivation.

INTRODUCTION

Healthy aging depends on the proper and persistent function of tissue-specific stem cell populations throughout the body.[1,2] Numerous studies have shown that a variety of genetic and environmental factors can contribute to dysfunction in stem cell maintenance and self-renewal, resulting in premature tissue aging.[3–7] The dormant state of cellular quiescence (G_0) is the primary mechanism by which premature proliferative exhaustion of stem cell populations is prevented with age.[8] Although often described simply as a state of reversible non-proliferation, recent discoveries suggest that the regulation of G_0 is remarkably diverse and dynamic.[9–12] The G_0 state allows stem cells to remain poised for reactivation. Upon receiving specific activation cues, stem cells rapidly reenter the cell cycle to produce differentiated progeny to restore and maintain tissue homeostasis.[13,14] In fact, several genes are upregulated during G_0, and knock-down studies have shown that these cell state-specific genes are required for preventing stem cell depletion, suggesting that G_0 is more tightly regulated than previously thought.[15–17] Yet, few studies have focused on evaluating whether stem cells during G_0 are molecularly equivalent and whether all G_0 stem cells undergo age-related changes. We anticipate the G_0 stem cell pool to change with age, and qualifying these changes will make it possible to accurately predict the regenerative capacity of tissues as they age.

Uncovering the extent and complexity of G_0 within mammalian stem cell populations and determining whether age-associated changes in these molecular programs occur *in vivo* remains challenging. However, melanocyte stem cells (McSCs) that exist within the hair follicle stem cell niche provide an ideal model to address this problem. McSCs are responsible for providing the differentiated, pigment-producing melanocytes that reside in the hair follicle bulb. These melanocytes deposit melanin into the growing hair follicle, which results in the coloration of our hair.[18,19] Gray hair is one of the most readily recognized and outwardly visible age-associated phenotypes. Graying has been largely attributed to the gradual depletion of McSCs with age and a failure to replenish the pool of melanocytes responsible for secreting melanin pigment into hair.[5,20] McSC activation and G_0 are easily evaluated because these processes are inextricably tied to distinct stages of the hair cycle. The hair cycle consists of three main stages: growth (anagen), regression (catagen), and dormancy (telogen). The timing and checkpoints of each of these stages have already been subject to extensive studies and characterization.[21]

[1]Department of Biology, University of Alabama at Birmingham, Birmingham, AL, USA
[2]NIH Intramural Sequencing Center, National Human Genome Research Institute, National Institutes of Health, Bethesda, MD, USA
[3]Genetic Disease Research Branch, National Human Genome Research Institute, National Institutes of Health, Bethesda, MD, USA
[4]Cancer Systems Biology, Institute of Diabetes and Cancer, Helmholtz Zentrum München, Ingolstädter Landstraße 1, 85764 München, Germany
[5]School of Life Sciences Weihenstephan, Technical University München, Maximus-von-Imhof-Forum 3, 85354 Freising, Germany
[6]Institute for Advanced Study, Technical University München, Lichtenbergstraße 2a, 85748 München, Germany
[7]Metaflux, San Diego, CA, USA
[8]Lead contact
*Correspondence: harrisml@uab.edu
https://doi.org/10.1016/j.isci.2024.110908

An enriched population of quiescent McSCs (qMcSCs) can be isolated from the telogen stage of the hair cycle using melanocyte-specific cell surface markers based on the fact that telogen hairs are devoid of proliferating and differentiated melanocytes.[4] This advantageous feature is inherent to the biology of the hair cycle in mice. It also allows us to uncover the underlying network of genes specifically upregulated by McSCs during G_0 in early adulthood, to identify essential biological processes associated with the transition of melanoblasts to qMcSCs, and to assess how this transcriptional state is maintained with age. Notably, we discovered that qMcSCs are enriched in genes associated with immune system processes, including the upregulation of the gene *Cd274*, which codes for the immune checkpoint programmed death-ligand 1 (PD-L1). Generally, binding of PD-L1 to its receptor, programmed death 1 (PD-1), promotes peripheral immune tolerance. However, our study reveals an additional and unexpected connection between PD-L1 and cellular quiescence. We also observed that qMcSCs expressing PD-L1 tend to persist with age while other qMcSCs are lost. This discovery could have implications for potential strategies to reverse age-related changes by reactivating the remaining PD-L1 expressing stem cells.

RESULTS

Defining the *in vivo* transcriptomes of quiescent melanocyte stem cells – from progenitor melanoblasts through adulthood, and toward dysfunction with age

To identify gene signatures that characterize qMcSCs during adulthood and with age, we isolated enriched populations of melanocytic cells from the dermis of female mice at three timepoints (Figures 1A and 1B). Actively proliferating stem cell precursors, or melanoblasts, were obtained from skins at postnatal day 0.5 (P0.5) when melanoblasts colonize the developing hair follicle. Adult and aged qMcSCs were obtained from skin synchronized in the telogen (dormant) hair stage at 8 weeks and 24 months old, respectively. We chose these adult and aged timepoints for their distinct differences in gray hair frequency, the latter being a readout of McSC dysfunction (Figure 1C). Cells were isolated from dissociated dermis using flow cytometry and $KIT^+/CD45^-$ selection, which specifically enriches melanocytic cells.[4,22] Enriched cells were subsequently processed for whole-transcriptome RNA sequencing (RNA-Seq) and differential gene expression analysis. We established two pairwise comparisons (Figure 1B) to identify differentially expressed genes (DEGs) filtered by the adjusted *p*-value ($p_{adj} < 0.05$) and fold change (absolute log2FC > 0.5): melanoblasts versus adult qMcSCs (8705 DEGs) and aged qMcSCs versus adult qMcSCs (916 DEGs; Data S1, Related to Figure 1).

Melanoblasts versus adult quiescent melanocyte stem cells

Transition to quiescence is an active transcriptional process

Comparing melanoblasts to adult qMcSCs via RNA-Seq yielded 8705 DEGs ($p_{adj} < 0.05$, absolute log2FC > 0.5). We interpret these DEGs as reflecting the global shift in gene expression required for actively proliferating melanoblasts to successfully colonize the hair follicle stem cell niche, acquire stemness, and transition to the adult G_0 state. Expectedly, melanoblasts show higher levels of expression for several cell cycle-related genes, such as *Mki67*, *Cdk2*, and *Cdk4*, and melanogenesis-related genes, *Dct*, *Mitf*, *Pmel*, *Tyr*, and *Sox10*, but low levels of expression for known stemness genes, including *Epas1*, *Hes1*, *Klf4*, *Klf10*, and *Sox9*, along with several genes associated with the regulation of G_0 in other stem cell populations, including *Cdkn1a*, *Nfatc1*, *Col12a1*, and *Arid5a* (Figure 1D). Further filtering the 8705 DEGs to the top 10% of the most highly expressed, up- and downregulated DEGs (based on the ranked expression of the normalized mean counts across samples) yielded 516 and 357 genes, respectively. The 516 highly expressed DEGs with elevated expression in melanoblasts over adult qMcSCs are referred to as the 'Melanoblast Core' gene signature, and the 357 highly expressed DEGs with depressed expression in melanoblasts compared to adult qMcSCs are referred to as the 'Adult qMcSC Core' gene signature (Data S1, Related to Figure 1). The 'Melanoblast Core' included well-known proliferation markers such as *Ki67* and *Top2a*, whereas the 'Adult qMcSC Core' included protein homeostasis (*Hspa1a*, *Hspa1b*) and adhesion genes (*Cadm2*, *Cdh2*, *L1cam*). Using gene set enrichment analysis (GSEA) to evaluate each core individually, the top 20 overrepresented biological processes associated with the 'Melanoblast Core' included mRNA metabolic processes, cytoskeletal organization, translational initiation, and RNA processing, while the 'Adult qMcSC Core' is characterized by regulation of transcription, cell differentiation, cell proliferation, and cell death as well as response to both abiotic and external stimuli (Figure 1E). Altogether, these initial results suggest that G_0 in McSCs is not an idle process and is instead actively maintained by various genes involved in several biological processes that underlie this dormant state. The high expression of G_0-specific genes and pathways seen within the 'Adult qMcSC Core' further demonstrates that G_0 in qMcSCs is not simply reflective of the downregulation of all major cellular processes.

Immune system processes, programmed death-ligand 1, and transcription factors are associated with adult quiescent melanocyte stem cells

To dissect key processes that drive or maintain stemness or G_0 in adult qMcSCs, we used functional connectivity analysis to highlight the interrelationship of the 'Adult qMcSC Core' DEGs. These genes resolved into five major branches connected by several hub genes (genes with an above-average number of interaction partners and is likely to play a regulatory role within the cell; Figure 2A). Enrichment analysis of these DEGs showed each branch representing unique biological processes: regulation of transcription, biological adhesion, regulation of the cell cycle, signaling and cell death, and immune system processes (Figure 2B). These branches mirror established processes involved in G_0 regulation, like 'biological adhesion' and 'regulation of cell cycle'. However, they also highlight novel processes, like the immune response, as integral components involved in the adult qMcSC state. For immune genes, these included key transcription factors *Stat3* (also a hub

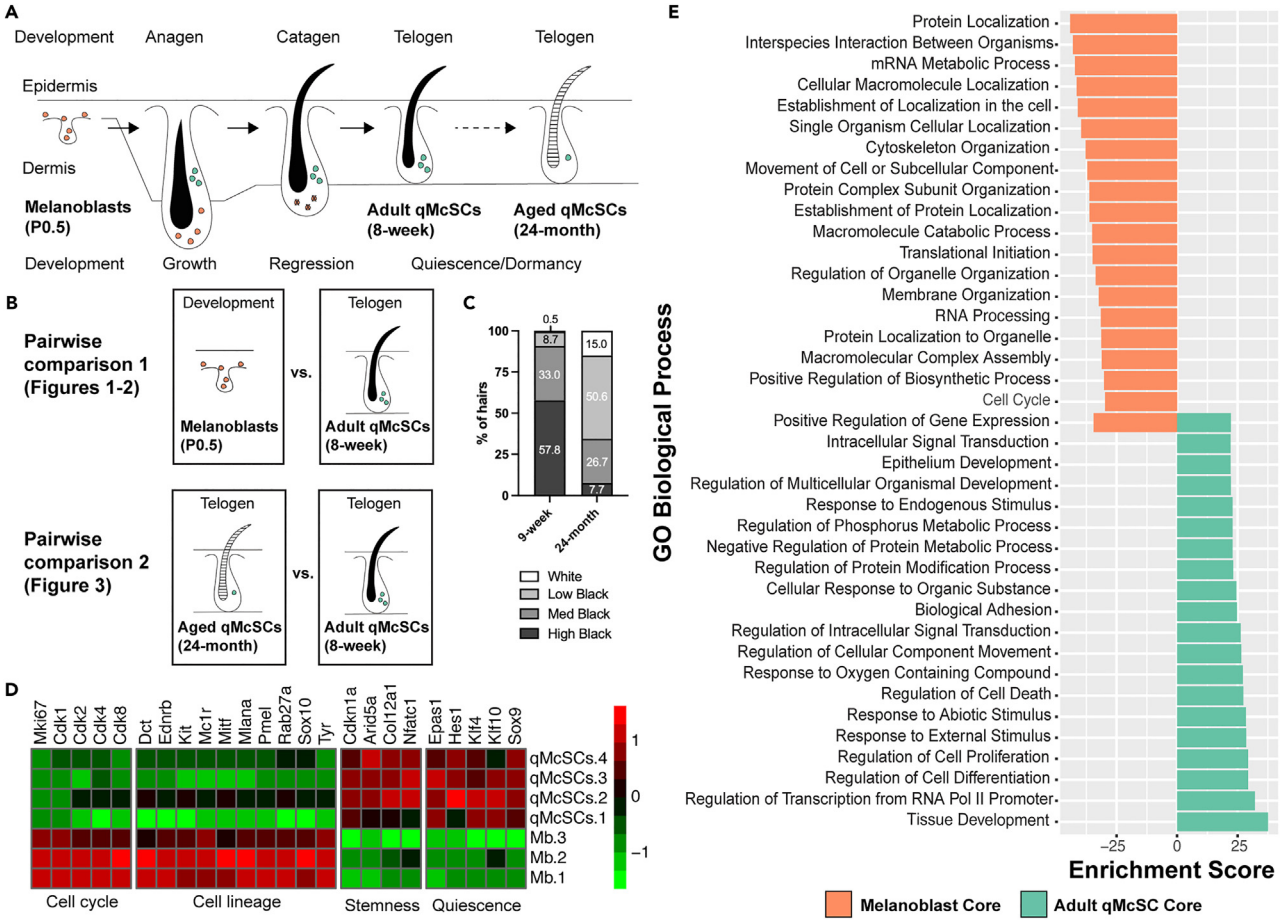

Figure 1. RNA-Seq comparison of melanocytic cells reveals novel pathways involved in melanoblast (Mb) and adult quiescent melanocyte stem cell (qMcSC) states

(A) Diagram depicting the spatiotemporal relationship of melanocytic cells with respect to distinct hair cycle stages (anagen, catagen, and telogen). Orange circles refer to melanoblasts and melanocytes, whereas teal circles refer to melanocyte stem cells (McSCs). Horizontal bars within the 24-month hair shaft represent the general process of hair graying.

(B) Graphical representation of the two pairwise comparisons of melanocytic cells evaluated in this study. Melanocytic cells are isolated using flow cytometric cell enrichment for KIT+/CD45-and evaluated using RNA-Seq (melanoblasts, n = 3 pooled samples; adult qMcSCs, n = 4 pooled samples; aged qMcSCs, n = 2 pooled samples). Pairwise comparison 1 corresponds to perinatal day 0.5 (P0.5) melanoblasts vs. 8-week-old, adult qMcSCs, and pairwise comparison 2 corresponds to 24-month-old, aged qMcSCs vs. 8-week-old, adult qMcSCs.

(C) Quantification of hair shaft pigmentation was compared between 9-week-old (n = 5) and 24-month-old (n = 4) mice using our established pigmentation binning method.

(D) Heatmap of selected cell cycle, cell lineage, stemness, and quiescence-associated differentially expressed genes (DEGs; $p_{adj} < 0.05$, absolute log2FC > 0.5) between P0.5 melanoblasts and 8-week-old adult qMcSCs.

(E) Clustered bar graph of the top 20 enriched biological processes associated with the 'Melanoblast Core' genes (orange, top 10% of the most highly-expressed DEGs with elevated expression in melanoblasts over adult qMcSCs) and 'Adult qMcSC Core' genes (teal, top 10% of the most highly-expressed DEGs with depressed expression in melanoblasts over adult qMcSCs).

gene), *Stat2*, *Irf1*, and *Irf9*, but also the immune checkpoint gene *Cd274*, referred to here as *Pd-l1*. The *Pd-l1* gene encodes the programmed death ligand 1 (PD-L1) protein and was of keen interest as PD-L1 participates in an immune-evasion mechanism that is co-opted in melanoma.[23,24] By RNA-Seq, *Pd-l1* is expressed by both melanoblasts (baseMean expression: 680.21) and qMcSCs (baseMean expression: 3598.35) yet is 5-fold higher in the latter (p_{adj} = 6.7E-22). Within the 'Adult qMcSC Core', not only was *Pd-l1* present but also *Egfr*, a signal receptor upstream of *Pdl1* transcriptional activation,[25] and several genes whose proteins are known to directly bind or regulate *Pd-l1*, including the hub genes *Stat3*, *Jun*, and *Myc*, along with the transcription factors *Irf1*, *Stat5a*, and *Stat2*.[26–28] Amongst these upstream regulators, the combined interaction scores between PD-L1 and EGFR, STAT3, and IRF1 (determined by the PPI parameters in STRING described in detail in the STAR Methods section) were found to be the strongest at 0.855, 0.845, and 0.708, respectively (Figure 2C). This observation highlights a potential mechanism involving EGFR, STAT3, and IRF1 in driving *Pd-l1* expression during G_0 induction in McSCs. Based on these

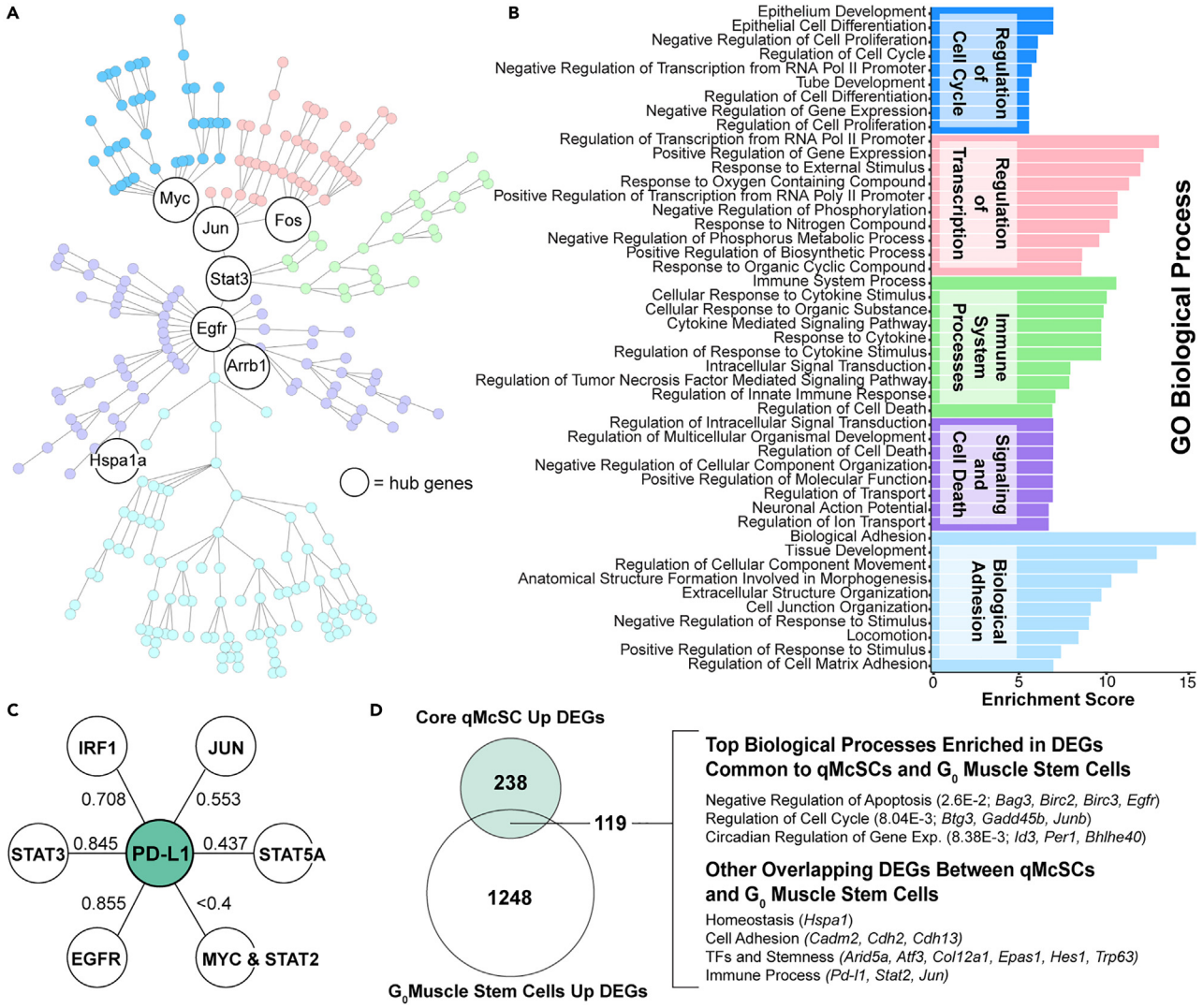

Figure 2. Upregulated immune system processes are characteristic of adult qMcSCs as well as G_0 muscle stem cells

(A) Protein-protein interaction network of the gene signature referred to as 'Adult qMcSC Core' reveals five major branches enriched for specific biological processes. Branches are color-coded by pathways matching the enrichment analysis in B. Hub genes, characterized by elevated branching, are highlighted by a larger node circle size.

(B) Clustered bar graph lists the top enriched biological processes for each of the five branches identified in panel (A).

(C) Combined interaction scores connect upstream regulators and common downstream effectors. *Pd-l1* (*Cd274* gene) is controlled by prominently upregulated 'Adult qMcSC Core' differentially expressed genes (DEGs), which are known to be *Pd-l1* gene promoter binding partners or are upstream of *Pd-l1* expression. Interaction scores were based on text-mining, experimental, and database evidence obtained from the STRING database (v11.0).

(D) Overlap of 'Adult qMcSC Core' DEGs and genes with elevated expression in G_0 muscle stem cells. Overlapping pathways and biological processes are listed with *p*-values and gene members common to both datasets.

observations, we hypothesize that immune system processes play an important role in qMcSCs and that *Pd-l1* is a marker and potentially a mediator of McSC function during G_0.

Programmed death-ligand 1 is also upregulated during quiescence in another stem cell population, namely muscle stem cells

Substantiating the broader relevance of our results, we asked whether the 'Adult qMcSC Core' DEGs overlap with one of the most studied G_0 stem cell populations, muscle stem cells. To answer this, we took advantage of a publicly available gene expression dataset comparing quiescent muscle stem cells that reside in a shallow dormant state, known as G_{Alert}, with quiescent muscle stem cells from a deeper dormant state, referred to simply as G_0.[29] Comparing these two states, 1367 genes are upregulated in G_0 versus G_{Alert} muscle stem cells ($p_{adj} < 0.05$, absolute L2FC > 0.5). Intersecting these upregulated G_0 muscle stem cell genes with our 'Adult qMcSC Core' DEGs showed an overlap of 119 common

between the two quiescent stem cell populations (Figure 2D). Enriched genes within this overlap represented the biological processes of 'negative regulation of apoptosis' (*Bag3*, *Birc2*, *Egfr*, and *Birc3*), 'regulation of cell cycle' (*Btg2*, *Gadd45b*, and *Junb*), and 'circadian regulation of gene expression' (*Id3*, *Per1*, and *Bhlhe40*). This overlap also included genes related to protein homeostasis (*Hspa1*), biological adhesion (*Cadm2*, *Cdh2*, and *Cdh13*), TFs, stemness (*Arid5a*, *Atf3*, *Col12a1*, *Epas1*, *Hes1*, and *Trp63*), and immune system processes (*Pd-l1*, *Stat2*, *Jun*; Figure 2D). Strikingly, *Pdl1* along with the TFs *Stat2* and *Jun* are expressed at elevated levels in both G_0 muscle stem cells and adult qMcSCs in comparison to their less quiescent counterparts. Comparing melanocyte and muscle stem cell populations suggests a common foundation that includes *Pd-l1* and other immune-related genes in the regulation of these stem cell populations, a role that has thus far been unappreciated.

Aged quiescent melanocyte stem cells versus adult quiescent melanocyte stem cells

The aging of qMcSCs is accompanied by an enhanced quiescence signature but not a senescence signature

Comparing aged qMcSCs to adult qMcSCs via RNA-Seq yielded 916 DEGs ($p_{adj} < 0.05$, absolute log2FC > 0.5). We interpret these DEGs as reflecting age-related changes that may dictate the regenerative potential of the qMcSC pool. Basic gene ontology analysis of the upregulated DEGs (256/916) showed low enrichment for a few broad cellular pathways (e.g., 'central nervous system development', 'response to external stimulus', 'biological adhesion'). Mirroring our previous terminology, the 256 DEGs with elevated expression in aged qMcSCs over adult qMcSCs we refer to as the 'Aged qMcSC Core' gene signature (Data S1, Related to Figure 3). The downregulated DEGs (660/916) showed high enrichment for a set of related processes, including translation, ribosome biogenesis, and protein trafficking (e.g., 'protein targeting to membrane', 'translational initiation', 'rRNA metabolic process') (Figure 3A). In order for inactive stem cells to be poised to reenter the cell cycle, they must strike a fine balance between lowering their translational activity while also maintaining adequate rRNA synthesis and ribosome biogenesis.[30] Therefore, the downregulation of genes involved in both protein synthesis and ribosome biogenesis may indicate that the aging of qMcSCs is associated with a deeper entrenchment into G_0 (also known as deep G_0).

Unlike other aged tissues, a senescence-associated secretory phenotype (SASP) is not prominently represented in the 'Aged qMcSC Core' and only a few DEGs expressed at high levels in aged qMcSCs overlapped with senescence gene lists (*Anapc15, Vgf, Serpine1, Krt78, Krt7, Itgax, Igf2, Hgfac,* and *C4a*). Notably, other members of the SASP are actually downregulated, including *Fas, Igfbp3,* and *Igfbp7,* and no change was observed in genes encoding other key SASP marker proteins like *Cdkn2a, Il6, Il1,* and *Cxcl8* (IL8), the matrix metalloproteinase (*Mmp*) gene family, the chemokine ligand (*Cxcl*) gene family, the cytokine (*Ccl*) gene family, or the metallopeptidase inhibitor (*Timp*) gene family.[31,32] DEGs between adult and aged qMcSCs also contained some overlap with known genes associated with aging (comparison made to the GenAge database[33,34]); these included the upregulated DEGs *Igf2*, *Serpine1*, and *Sstr3,* and the downregulated DEGs *Fas, Igfbp3, Lepr, Ngfr, Nr3c1, Prkca,* and *Stk11*. A number of these genes participate in the regulation of metabolism, with the upregulation of *Igf2* along with the downregulation of *Igfbp3* and *Stk11* suggesting enhanced mammalian target of rapamycin (*mTOR*) signaling.[35,36] Altogether, these observations demonstrate that G_0 in McSCs is not immutable, and is uniquely affected by age, and this intrinsic aging process is likely SASP-independent. Interestingly, however, the transcriptional changes accompanying aging in qMcSCs suggest two potentially conflicting biological processes: reinforced G_0 on the one hand and an apparent requirement for the metabolic regulator mTOR for McSC maintenance on the other hand.

Aged quiescent melanocyte stem cells do not revert to a melanoblast or differentiation gene signature

To understand how the 916 DEGs identified from our RNA-Seq comparison of aged qMcSCs to adult qMcSCs changed over time, we used a cross-sectional approach to examine these genes across the three RNA-Seq timepoints evaluated in this study; P0.5 (melanoblast), 8-week (adult qMcSC), and 24-month (aged qMcSC). Within our cross-sectional data, we focused on six distinct patterns of expression (Figure 3B; Data S2, Related to Figure 3): 236/916 DEGs reverted to a more melanoblast-like expression level compared to adult qMcSCs (patterns I-II); 411/916 DEGs appeared when transitioning from adult to aged qMcSCs (patterns III-IV); and 269/916 DEGs showed either progressive up- or down-regulation with age (patterns V-VI). Given that one phenotype of aged McSCs in both mice and humans is premature differentiation,[20] we were particularly interested in addressing whether qMcSCs exhibit any signature indicative of this process. We focused first on 'reversion to melanoblast-like expression' (pattern II) because we anticipated these DEGs might reveal a return to a melanoblast level of melanocyte differentiation markers that were lost when these cells acquired stemness. However, of the 14 DEGs that were higher in both melanoblasts and aged qMcSCs compared to adult qMcSCs (pattern II), none were pigmentation related nor enriched for any particular pathway. DEGs with low expression in both melanoblasts and aged qMcSCs (pattern I) were interpreted as important drivers of the G_0 and stem cell states in adult McSCs that are lost with age. These DEGs were enriched for the processes of early neural crest cell differentiation (*Sfrp, Gdnf, Nrp2, Cdh2, and Sema3e*) and mechanisms for cell junction assembly (*Reln, Col17a1, Cdh2, Mpp7, Plec, Itgb4, Tns1, and Pecam1*) and cell-cell adhesion (*Pcdh1, Mpz, Tenm1, Pcdh17, Pcdh10, Ecm2, Lrrc4c, Cadm4, Arvcf, and Adgrl3l*). Taken together, gene ontology analysis of the DEGs within the 'reversion to melanoblast-like expression' patterns (I, II) points to dysregulation of pathways potentially involved in stemness and the structure of the stem cell niche, but not McSC differentiation, as characteristics of aging in McSCs during dormancy.

Enrichment for opposing cell processes suggests heterogeneity in the quiescent melanocyte stem cell pool

Of the remaining patterns, 'age-specific decrease of expression' (pattern IV) and 'progressive loss of expression with age' (pattern V) highlight a dichotomy within our gene expression data (Figure 3C). Pattern IV is enriched for genes suggesting that aged qMcSCs may be less G_0 and

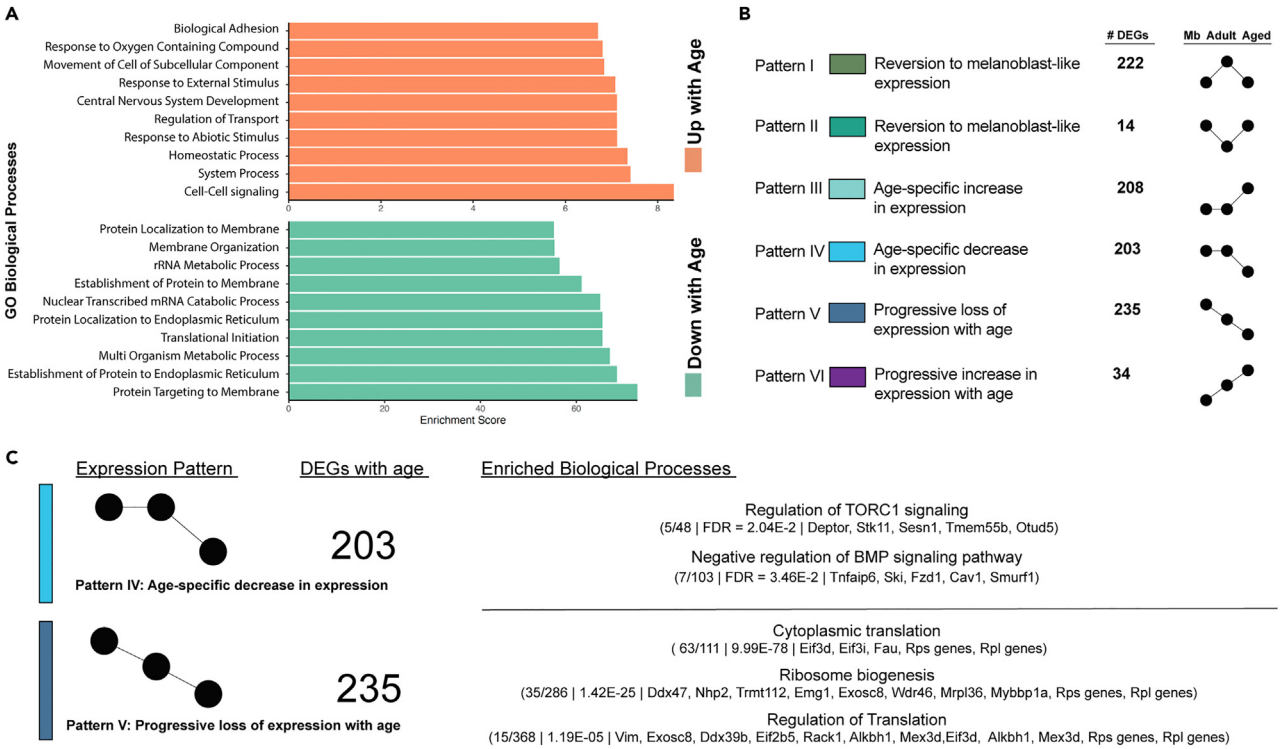

Figure 3. RNA-seq reveals a transcriptional shift accompanying qMcSC aging

(A) Clustered bar graph shows biological processes identified by gene set enrichment analysis of the differentially expressed genes (DEGs) from the comparison of aged qMcSCs to adult qMcSCs by RNA-Seq.

(B) DEGs identified by comparing aged qMcSCs to adult qMcSCs were viewed across three timepoints; melanoblast (P0.5), adult (8 weeks), and aged (24 months). Gene expression across this time course is represented by six select patterns (I-VI) shown using ball-and-stick diagrams. The number of DEGs for each pattern is indicated.

(C) A structured list of representative biological processes and genes, including enrichment and false discovery rate (FDR) for each signature, along with gene symbols of significantly regulated transcripts.

more prone to loss of self-renewal compared to their more youthful qMcSC counterparts. For instance, this pattern IV category shows decreased levels of the mTOR inhibitors *Deptor, Stk11,* and *Sesn*. The activity of mTOR defines different states of G_0; higher levels are associated with more 'alert' G_0 stem cells that can respond rapidly for tissue repair, while lower levels are associated with 'deep' G_0 stem cells that are kept in reserve.[29] Pattern IV also shows decreased levels of the bone morphogenetic protein (BMP) signaling inhibitors *Ski, Cav1,* and *Smurf1*. During pigment regeneration, BMPs are not necessary for the maintenance of qMcSCs yet they are essential for proper maturation of committed McSC progeny.[37] Conversely, within pattern V we observe that genes whose expression is progressively lost with age are enriched for translation and ribosome biogenesis pathways similar to those highlighted in Figure 3A. For pattern V genes, our cross-sectional approach revealed that the downregulation of protein synthesis is not unique to the transition between adult and aged qMcSCs but instead is a further reinforcement of the G_0 process acquired during the initial establishment of qMcSCs from melanoblasts. Functional heterogeneity of the McSC pool has been observed previously and could explain these conflicting observations.[38,39] Our recent high-resolution single-cell RNA-Seq confirms that qMcSCs can be divided into several subpopulations when compared transcriptomically and supports the possibility that our data here reflects two independent populations of qMcSCs with different potentials that are also affected by age differentially.[40]

Programmed death-ligand 1 expression marks a subpopulation of quiescent melanocyte stem cells in vivo that is retained with age

To validate the increased transcript abundance of *Pd-l1* by qMcSCs during G_0, we assessed PD-L1 protein expression during the dormant (telogen) hair stage in the skin of adult PD-L1 wildtype (WT) and knockout (KO) mice (2–3-month-old males and females; C57BL6-*Cd274*^{tm2Shr}, gift from Arlene Sharpe). KO animals were included in this evaluation to distinguish real PD-L1 expression from non-specific antibody staining; any immunoreactivity observed in WT skins that is lost in PD-L1 KO skins should represent tissues that truly express PD-L1. Dopachrome tautomerase (DCT) was utilized as a protein marker for McSCs. During telogen, anti-PD-L1 immunoreactivity in PD-L1 WT animals showed prominent staining in the inner layer of the hair bulge, the sebaceous gland (SG), and in some DCT+ qMcSCs in the outer layer of the hair bulge

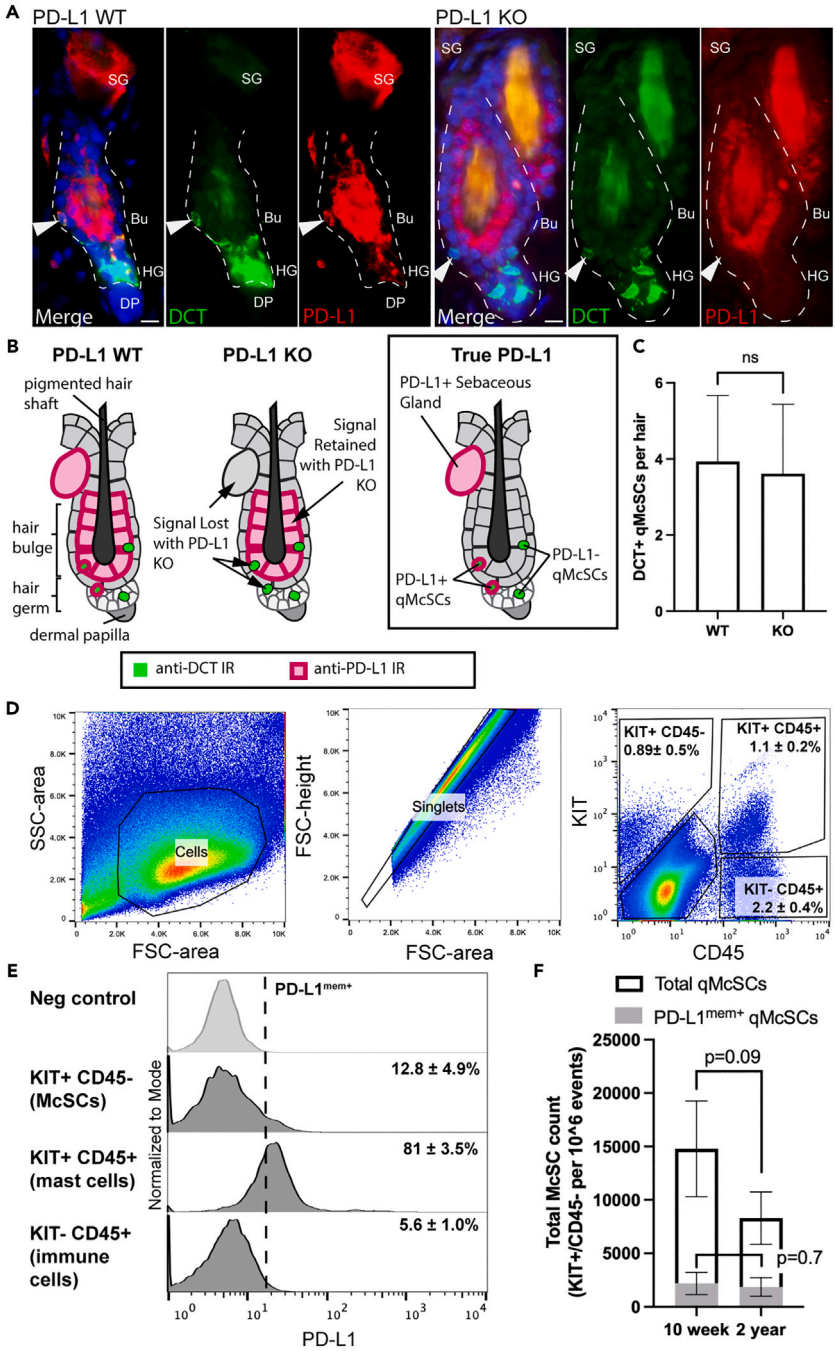

Figure 4. PD-L1 is expressed by both adult and aged qMcSCs *in vivo*

(A) Representative images showing PD-L1 immunoreactivity (red) in the hair follicle and in qMcSCs (DCT, green) during the telogen (dormant) stage of the hair cycle in skins from 2-3-month-old PD-L1 WT and KO specimens irrespective of sex. Tissues were counterstained with DAPI (blue). Arrowheads mark McSCs. Dotted lines highlight the shape of the hair follicles. Abbreviations: Bu, bulge; HG, hair germ; SG, sebaceous gland; DP, dermal papilla. The scale bar represents 10 μm.

(B) Summary diagram depicting the immunoreactivity (IR) observed in PD-L1 WT and KO mice, highlighting the subtractive pattern that reveals "true PD-L1" expression associated with telogen hairs.

(C) Quantification of DCT+ qMcSCs in skins of PD-L1 WT (n = 63 hairs across 3 animals) and KO (n = 80 hairs across 4 animals) animals immunolabeled as in (A).

(D) KIT and CD45 gating strategy for the isolation and quantification of qMcSCs (KIT+/CD45-), mast cells (KIT+/CD45+), and other immune cells (KIT-/CD45+) (n = 4). Refer to Figure S2 for gating controls.

Figure 4. *Continued*

(E) Representative histograms of PD-L1 expression and the fraction of PD-L1^{mem+} cells within the KIT/CD45 subpopulations indicated in panel B. Membrane-specific PD-L1 expression is determined by positive staining on the surface of live, non-permeabilized cells. The percentage of PD-L1^{mem+} cells for each population is shown (mean ± SD, $N = 4$).

(F) Quantification of PD-L1^{mem+} qMcSCs in the dissociated dermis from adult (10-week-old) and aged (24-month-old) female mice ($n = 3$ per time point), determined by flow cytometry. In column graphs, bars represent the mean ± SD. Significance as determined via T-test and the *p*-values are indicated.

(Figure 4A; Figure S1, Related to Figure 4). PD-L1 immunoreactivity was also present within the hair germ and sometimes overlapped with DCT+ qMcSCs, but this was variable. With PD-L1 KO, we consistently only observed PD-L1 immunoreactivity in the inner layer of the hair bulge (Figure 4A; Figure S1, Related to Figure 4). Based on this subtractive expression pattern, we consider the staining observed in the SG, and the DCT+ qMcSCs within the hair bulge and hair germ of PD-L1 WT mice reflective of actual tissues that express PD-L1 protein. We interpret the staining of the inner layer of the hair bulge as an artifact associated with this IHC method and the PD-L1 antibody (Figure 4B). These observations are consistent with previous evaluations of PD-L1 staining in mouse skin, which corroborates PD-L1 localization to the sebaceous gland but did not closely evaluate PD-L1 expression by McSCs.[41] Within these same skins we also took advantage of evaluating the effects of PD-L1 KO on the qMcSC population. There was no significant difference in the average number of DCT+ qMcSC per hair when comparing PD-L1 WT and KO mice suggesting the role of PD-L1 in these cells is for something other than maintaining the abundance or survival of the qMcSC pool at this time point (Figure 4C).

Because not all qMcSCs appeared PD-L1 positive by immunohistochemistry, we quantitatively assessed qMcSCs for PD-L1 expression using flow cytometry. We focused here on highlighting membrane-associated PD-L1 (PD-L1^{mem+}) expression on the surface of non-permeabilized cells, as this is where PD-L1 exerts its cellular function. Using the same KIT/CD45 isolation strategy described above, we detected just under 1.0% of KIT+/CD45- McSCs, just over 1.0% of KIT+/CD45+ mast cells, and ~2.2% of other KIT-/CD45+ immune cells in the dermis of telogen stage, 8-week-old adult mice (Figure 4D; Figure S2, Related to Figure 4). Based on gating above the background of non-stained cells, a portion of KIT+/CD45- McSCs expressed PD-L1^{mem+} (12.0 ± 4.9%), as did the majority of KIT+/CD45+ mast cells (81.0 ± 3.5%) and some of the other KIT-/CD45+ immune cells (5.6 ± 1.0%). The latter two groups are known to express PD-L1 physiologically and serve as positive controls (Figure 4E).[42,43] The specificity of this PD-L1 antibody for flow cytometry was confirmed by others after *Pd-l1* knockout and IFNγ induction.[44,45] Our recent evaluation of qMcSCs by single-cell RNA-Seq further corroborates these findings by demonstrating that two independent clusters of qMcSCs are characterized by elevated *Pd-l1* gene expression.[40] Single-cell RNA-Seq of the hair follicle also corroborates the positive staining we observe in the sebaceous gland.[46] These results indicate that PD-L1 is not only expressed at the cell membrane of immune cells within the dermis but also by some non-immune cells including qMcSCs.

These results show that PD-L1 expression can be used as a marker to identify a subpopulation of qMcSCs *in vivo* that exists in early adulthood and parallels the upregulation of *Pd-l1* gene expression observed in the 'Adult qMcSC Core' dataset. Interested in further understanding how PD-L1^{mem+} expression changes in qMcSCs with age, we evaluated qMcSCs isolated from young (8-week) and aged (24-month) mice. In comparison to the pool of young qMcSCs, aged qMcSCs were reduced by almost half, yet the proportion of PD-L1^{mem+} qMcSCs was retained (Figure 4F). The overall reduction of McSCs with age is consistent with the canonical, age-related stem cell loss pathway, but our data suggests PD-L1^{mem+} qMcSCs appear to be resistant to this process.

Developing a method to evaluate the association of programmed death-ligand 1 with quiescence using melanoblasts *in vitro*

Immortalized melanoblasts can be used to model quiescence and cell cycle reentry

To attribute relevance to PD-L1^{mem+} expression by qMcSCs *in vivo*, we next investigated whether increased PD-L1 is associated specifically with quiescence rather than stemness. To test this possibility, we used the *in vitro* culture method of serum deprivation and mitogen withdrawal to specifically induce G_0 in a non-stem, melanoblast cell line. During development, qMcSCs derive from embryonic and perinatal melanoblasts that colonize the hair follicle during hair follicle morphogenesis, and melb-a cells are an immortalized, non-differentiated line of melanoblasts isolated from neonatal skin.[47] For this G_0 induction method, cells are synchronized to the G_1 phase of the cell cycle using mitogen withdrawal. Mitogen withdrawal is executed by removing stem cell factor (SCF) and basic fibroblast growth factor (bFGF) for one day, followed by reducing serum from 10% to 0.1% to induce G_0 and then evaluated using flow cytometry. 5-ethynyl-2′-deoxyuridine (EdU) labeling, which is widely used to visualize cells actively synthesizing DNA,[48] demonstrates that two days of serum deprivation (aka, 2-day G_0 cells) is sufficient to stall melb-a cells in the G_0/G_1 stages of the cell cycle. This contrasts with actively proliferating melb-a cells grown in media with mitogens and 10% serum ('active cells'), which are found distributed across all stages of the cell cycle, including the S phase (Figure 5A). Immunofluorescent staining showed that 2-day G_0 cells also downregulate the classic cell cycle and proliferation marker *Mki67* with 2-day G_0 cells exhibiting roughly 50% of the MKI67+ cells observed in active cells (Figure 5B). Since G_0 is defined by reversible arrest, we confirmed the ability of 2-day G_0 cells to re-enter the cell cycle as confirmation of our G_0 methods. To achieve this, we reintroduced the required growth factors for proliferation (mitogens plus 10% serum) to 2-day G_0 cells and used EdU to measure cell cycle reentry. By 18 h post-activation, reactivated 2-day G_0 cells are distributed across all phases of the cell cycle, with a similar percentage of cells in the S- and G2/M-phase of the cell cycle (total EdU+ cells) when comparing reactivated 2-day G_0 (45.6%) to active cells (50.6%). Further analysis showed that in reactivated 2-day G_0 cells, the majority of EdU+ cells are concentrated in the S-phase of the cell cycle, a clear indication that G_0 melb-a cells quiesced using our conditions can successfully reenter the cell cycle.

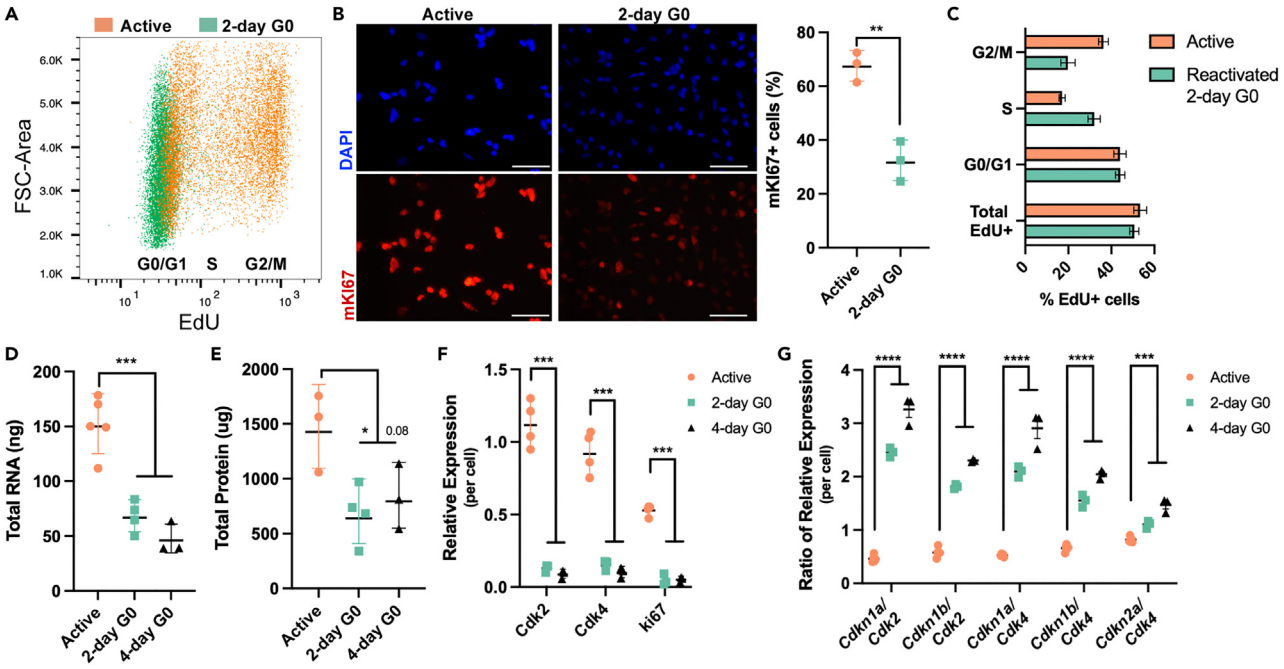

Figure 5. Immortalized melanoblasts (melb-a cells) can be quiesced and reactivated

(A) Representative scatterplot shows EdU labeling of actively proliferating (active, orange) and quiescent (2-day G_0, green) melb-a cells. The cell cycle state is indicated.

(B) Representative images of actively proliferating (active) and quiescent (2-day G_0) melb-a cells stained for DAPI (blue) and MKI67 (red), and associated quantification of the fraction of MKI67+ cells assessed by flow cytometry.

(C) The reactivation rate is determined by the fraction of dividing cells incorporating EdU 18 h post-reactivation over total cells. The reactivation rate is compared between 2-day G_0 and actively proliferating melb-a cells. Total EdU+ cells encompass only those cells in the G2/M or S phases.

(D and E) Quantification of total RNA (D) and protein (E) from in $1x10^6$ cells melb-a cells that are actively proliferating, 2-day G_0, or 4-day G_0.

(F) qRT-PCR quantification shows decreased relative expression of proliferation markers (*Cdk2*, *Cdk4*, and *Mki67*) in 2-day G_0 and 4-day G_0 melb-a cells compared to actively proliferating melb-a cells.

(G) qRT-PCR quantification of cyclin-dependent kinase inhibitors and respective CDKs represented as a ratio. In column graphs, each dot represents a biological replicate, and bars represent the mean ± SD. Significance as determined via T-test and asterisks indicate adjusted *p*-values (* <0.05, ** <0.01, *** <0.001, **** <0.0001).

(Figure 5C). Taken together, these results support the use of this *in vitro* mitogen withdrawal plus serum deprivation method to evaluate the nature of G_0 using the melb-a cell line.

Immortalized melanoblasts show classic markers of G0

Generally described as a static state of inactivity, cells suspended in G_0 show downregulation of several molecular processes, including DNA, RNA, and protein synthesis.[49,50] In comparison to active melb-a cells, 2-day G_0 cells exhibit significant reductions in their total RNA and protein levels, with actively proliferating cells having roughly two times the total RNA and protein content compared to G_0 cells. This low level of RNA and protein remains relatively consistent even if G_0 is extended to 4 days, suggesting that the G_0 program is likely established within the initial 2-day time frame (Figures 5D and 5E). We further characterized this G_0 program by evaluating the expression of cell cycle genes using qRT-PCR. Two major assumptions are generally made with regard to qRT-PCR experiments: (i) that only a small number of genes are changed between the two sample conditions, and (ii) that the overall size of the transcriptome (RNA content) remains constant across sample conditions.[51] We show this is not the case for both assumptions. To address these issues, we normalized the mean gene expression values by cell number rather than a standard housekeeping gene; the total cell number required to generate 1 μg of RNA was determined by cell sorting. Using this method, 2-day, and 4-day G_0 cells exhibit significant reductions in the expression of the early cell cycle activator genes *Cdk2* and *Cdk4*, as well as *Mki67* (Figure 5F). Conversely, genes for the known inhibitors of CDKs, *Cdkn1a* (P21), *Cdkn1b* (P27), and *Cdkn2a* (P16) show an increased ratio of expression when compared to their respective interaction partners. As the length of G_0 was extended, we observed a significant increase in the ratio of *Cdkns* to *Cdks* in 4-day G_0 cells compared to 2-day G_0 cells, suggesting that increased lengths of G_0 might alter the rate at which these cells reenter the cell cycle and proliferate (Figure 5G). In line with our EdU staining, these results indicate that melb-a cells grown in G_0 media are indeed quiescent; they exhibit classic markers of G_0 and have decreased expression of cell cycle genes but retain the ability to reenter the cell cycle when appropriate conditions are present.

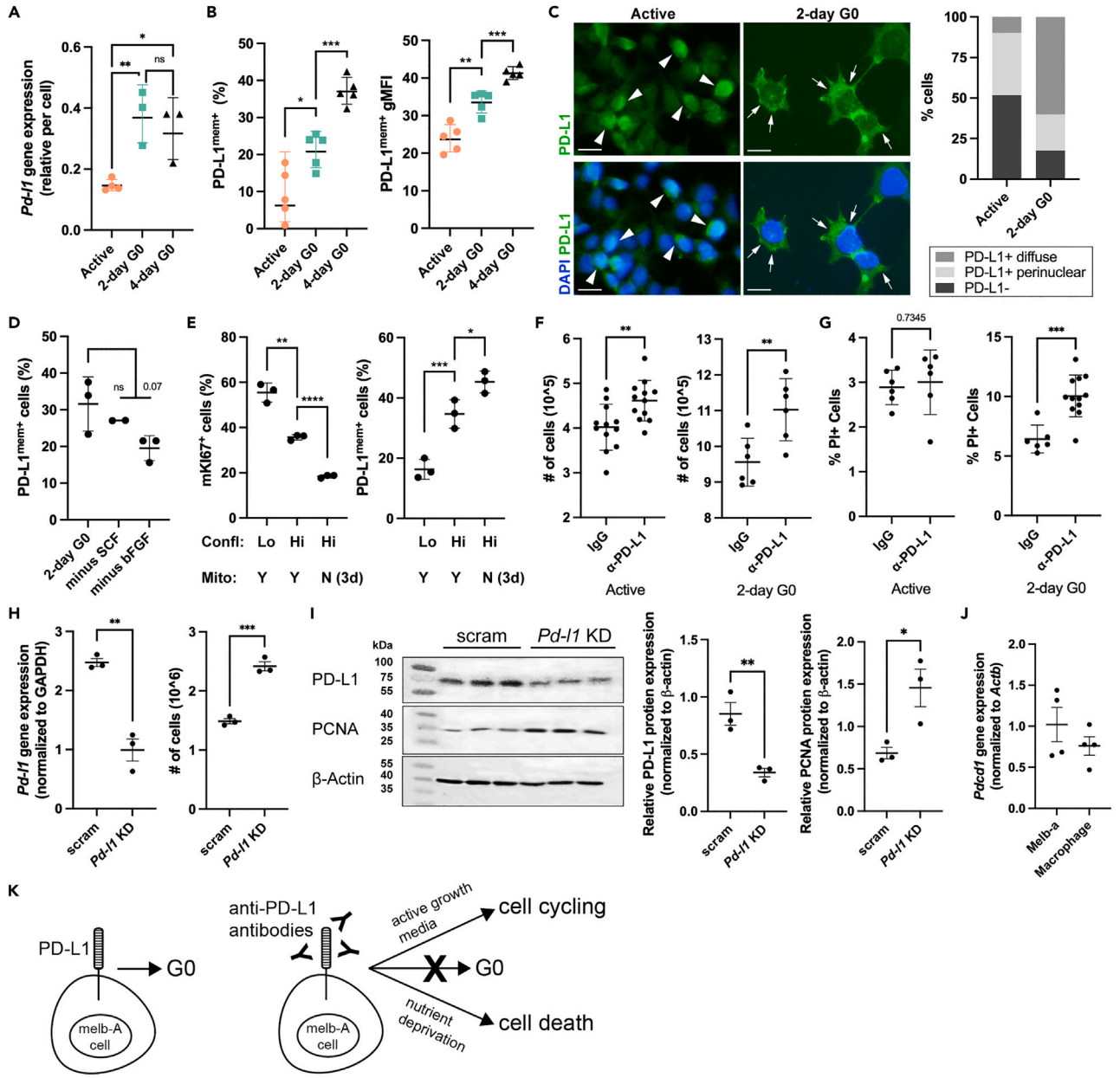

Figure 6. *Pd-l1* expression is a component of melanoblast quiescence and plays a functional role in melanoblast cell cycling dynamics

(A) qRT-PCR quantification showing increased relative expression of *Pd-l1* following G_0 induction of melb-a cells at 2- and 4-day G_0.

(B) Quantification of membrane-associated PD-L1 (PD-L1^{mem+}) expression on actively proliferating, 2-day G_0, and 4-day G_0 melb-a cells using flow cytometry. Membrane-specific expression is determined by positive staining on the surface of live, non-permeabilized cells. Comparison with the time course of the experiment shows a stepwise, significant increase in the fraction of PD-L1^{mem+} cells and PD-L1^{mem+} geometric mean fluorescent intensity (gMFI) with the length of G_0.

(C) Representative images of actively proliferating and 2-day G_0 melb-a cells stained for DAPI (blue) and PD-L1 (green) after fixation and permeabilization. Two different PD-L1 expression patterns emerge, one that is perinuclear and prevalent in actively proliferating melb-a cells, and one that is cytoplasmic and/or membrane associated (diffuse) and more prevalent in 2-day G_0 melb-a cells. The bar graph represents the associated quantification of observed staining patterns.

(D) Quantification of the percent of PD-L1^{mem+} cells with the removal of both mitogens (SCF and bFGF, 2-day G0) or single mitogens (SCF or bFGF) during entry into G_0.

(E) Quantification of the percentage of MKI67+ and PD-L1^{mem+} cells when using high confluency as an alternative method for inducing G_0.

(F) Quantification of cell number after treating active or G0-induced melb-a cells with non-specific control (IgG) or anti-PD-L1 antibody.

Figure 6. *Continued*

(G) Quantification of PI + staining measured by flow cytometry after treating active or G_0-induced melb-a cells with non-specific control (IgG) or anti-PD-L1 antibody.

(H) qRT-PCR quantification of *Pd-l1* gene expression (left) or cell number (right) after treatment with scramble (scram) or *Pd-l1* (*Pd-l1* KD) siRNA.

(I) Overlaid Western blot images demonstrating PD-L1, PCNA, and β-ACTIN protein expression after transfection of melb-a cells for 72 h with scramble (scram) or *Pd-l1* (*Pd-l1* KD) siRNA along with the corresponding protein standards. Graphs show relative protein expression levels (normalized to β-ACTIN) based on quantitative densitometry of the protein bands from immunolabeling and were measured in blot images without the protein standard overlay.

(J) qRT-PCR quantification showing detectable expression of the *Pdcd1* gene in active melb-a cells and macrophages (Raw264.7). Macrophages are known to express basal levels of *Pdcd1* and were used as a positive control.

(K) Diagram depicting the association of PD-L1^{mem+} expression with G0 in melb-A cells and the possible responses of these cells to blocking PD-L1^{mem+} with anti-PD-L1 antibodies. In column graphs, each dot represents a biological replicate, and bars represent the mean with standard deviation. Significance as determined via T-test and asterisks indicate adjusted *p*-values (* <0.05, ** <0.01, *** <0.001, **** <0.0001).

Elevated programmed death-ligand 1 is a physiological component of quiescence in melanoblasts

The expression of programmed death-ligand 1 by quiescent melanocyte stem cells suggests its role in the melanocytic lineage during quiescence

Having established the G_0 nature of melb-a cells after growth in G_0 media and confirming their ability to reactivate and re-enter the cell cycle, we next asked whether these cells also upregulate *Pd-l1* RNA and PD-L1 protein like that observed in qMcSCs *in vivo*. Akin to our RNA-seq results, we find that *Pd-l1* gene expression is significantly increased in 2- and 4-day G_0 cells compared to active cells (Figure 6A). Using flow cytometry, we find that PD-L1 at the cell membrane increases as active cells transition to G_0 cells; 2-day G_0 cells exhibit a significant increase in the percentage of cells expressing PD-L1^{mem+} and in the geometric mean fluorescence intensity (gMFI) of PD-L1^{mem+} cells over actively proliferating cells (Figure 6B). Interestingly, both the percentage and gMFI of PD-L1^{mem+} cells continue to increase with the length of G_0 (Figure 6B, comparing 2-day and 4-day G0). By immunocytochemistry, PD-L1 protein is clearly expressed by both active and 2-day G_0 cells yet undergoes a change in subcellular localization. In active cells, PD-L1 appears perinuclear. This switches to a more diffuse membrane and/or cytoplasmic localization upon G_0 induction. Quiescent conditions also induced increased cell spreading, a common morphological change associated with G_0 cells (Figure 6C). These *in vitro* observations parallel our *in vivo* discovery that PD-L1^{mem} is expressed by some qMcSCs (Figure 4). Altogether, these data highlight the importance of the spatial positioning (at the cell membrane) and timing (during quiescence) of PD-L1 expression for it to play a functional role during G_0 in cells of the melanocyte lineage.

A number of morphological and molecular characteristics demonstrate that G_0 regulation varies depending on the type of cells being studied and the conditions used to induce G_0.[10,13,52] For instance, our *in vitro* method for inducing G_0 in melb-a cells involves withdrawing the mitogens SCF and bFGF followed by serum deprivation (2-day or 4-day G0). During hair cycling *in vivo*, SCF is diminished during telogen and peaks around the proliferating hair bulb during anagen.[53,54] This suggests that loss of SCF may be a key factor in regulating G_0 in this context, and we were curious to know whether our *in vitro* model reflects this requirement. Indeed, removing just one mitogen at a time during G_0 induction *in vitro* indicated that withdrawal of SCF, but not bFGF, is sufficient to induce a similar percentage of PD-L1-expressing cells as with full mitogen withdrawal (Figure 6D). Additionally, G_0 induction using contact inhibition (cells grown at high confluency in 0.1% serum and in the presence of SCF and bFGF) resulted in a similar, though less pronounced, inverse relationship between PD-L1^{mem+} and MKI67 expression (Figure 6E). Altogether, these observations indicate that endogenous PD-L1 expression is associated with G_0 in the melanocyte lineage both *in vivo* and *in vitro* and may rely predominately on SCF removal. Our *in vitro* work also demonstrates that the change in PD-L1 expression observed upon G_0 induction is not unique to the method by which it is initiated but rather is a feature of G_0 in these cells.

A role for programmed death-ligand 1 within the melanocyte lineage beyond tumor-immune privilege

Despite much of the focus on PD-1/PD-L1 engagement in mediating tumor immune tolerance, PD-L1 can also transduce signals intrinsically that promote tumor progression and this can occur independent of PD-1 binding.[55–57] Antibodies that target PD-L1 can ameliorate intracellular PD-L1 signaling by inducing receptor internalization. With this idea in mind, and since a portion of both active and G0 cells express PD-L1 at the cell membrane (Figure 6B), we compared how active melb-a cells or those entering G0 respond to blocking autonomous PD-L1 signaling. Compared to non-specific, isotype-matched IgG, several days of treatment with anti-PD-L1 antibody resulted in a significant increase in cell number in both active and cells transitioning to G0 (Figure 6F). Propidium iodide (PI) staining showed that G0 cells experience an increase in cell death when treated with anti-PD-L1 antibody, while active cells appear unaffected (Figure 6G). Similarly, an increase in cell number is also observed when *Pd-l1* is knocked down using *Pd-l1*-targeted DsiRNA (Dicer-substrate short interfering RNA; Figure 6H). *Pd-l1* knockdown resulted in a significant decrease in PD-L1 protein expression with an associated increase in PCNA protein expression, indicating that the increase in cell numbers observed with *Pd-l1* knockdown is due to more cells undergoing cell division (Figure 6I). We detect little to no expression of the PD-1 gene, *Pdcd1*, in primary melanoblasts or qMcSCs by bulk RNA-seq (Data S1, Related to Figure 1) and we presume these *in vitro* effects are due to PD-L1 functioning independent of binding to its receptor PD-1. However, by qRT-PCR, melb-a cells do express low but detectable levels of the PD-1 gene, *Pdcd1*, thus we cannot rule out a contribution of PD-1 to these results at least in this context (Figure 6J). Nevertheless, these data support a functional role for PD-L1^{mem} in restricting cell cycling in melb-A cells. PD-L1^{mem} also prevents cell death of melb-A cells under quiescent conditions, which may reflect a direct role for PD-L1 in cell survival during quiescence induction or this cell death may be a consequence of being unable to enter the quiescent state when deprived of nutrients (Figure 6K). This data

counterbalances the body of work attributing PD-L1 exclusively to a pharmacological effector role in cancer and highlights that PD-L1 carries an underappreciated, physiological importance in non-tumorigenic cells during G_0.

DISCUSSION

In this study, transcriptomic profiling demonstrates that quiescent stem cells are not simply transcriptionally suppressed versions of their active counterparts but rather express genes to promote, maintain, and protect the G_0 state. With age, this control is altered, and the qMcSC pool as a whole appears more dormant than observed in youth. Of the genes associated with this process, *Pd-l1* is upregulated in a portion of qMcSCs and likely confers unique qualities to these cells.

Depletion of the McSC pool with age is considered the primary cause of gray hair.[20] However, the phenomenon that gray hair can be reversed suggests that not all McSCs are lost with age.[58] In mice, beginning at 12 months of age, the maximal length of the telogen stage of the hair cycle gradually increases by up to 32% during a process known as telogen retention.[59–61] A consequence of telogen retention is that McSCs are suspended in the G_0 state for increasing lengths of time with age. Previous studies also suggest that the length of G_0 can affect G_0 depth and the ability of G_0 cells to reenter the cell cycle.[11] Several studies have shown that the ability of aged stem cell populations to regulate the transition between G_0 and proliferation declines with age.[8,62,63] Reduced frequency of stem cell reactivation and tissue regeneration further contributes to the deterioration of tissue integrity and function overtime.[64,65] A deeper state of G_0 has been used to describe the reduced reactivation rate and prolonged re-entry into the cell cycle of several aged populations of cells *in vivo* including hepatocytes after partial hepatectomy, salivary gland cells after administration of isoproterenol, and muscle stem cell populations following a wounding event.[66–69] However, studies involving parasymbiosis reveal that entrenchment into G_0 may not necessarily be irreversible as the ability to restore tissue homeostasis is retained in several aged cell populations (hepatic, muscle, and neural) that fail to activate appropriately under normal physiological conditions within an aged environment.[70–72] *In vitro* studies on rat embryonic fibroblasts may explain why this is the case as holding cells in G_0 for increasing lengths requires a stronger stimulating signal in order to reactivate at a rate comparable to cells in a shallower G_0 state.[11] Recent work utilizing an elegant combination of lineage mapping and volumetric imaging analysis substantiates the idea that the McSC pool is comprised of stem cells with varying capacities to activate with hair cycling. Indeed, with repeated plucking, which mimics aspects of aging, the McSC pool becomes more dormant, and these dormant McSCs do not give rise to differentiated progeny.[73] These observations align with our evaluation of aged qMcSCs and point to changes in the depth of G_0 within the qMcSC population as a whole as a novel characteristic of melanocyte stem cell aging.

We show that *Pd-l1* is upregulated in qMcSCs in comparison to perinatal melanoblasts, and others have shown that *Pd-l1* is subsequently downregulated as qMcSCs activate, divide, and transition into differentiated McSC progeny.[37] These observations indicate that *Pd-l1* is dynamically expressed *in vivo* in association with cell state, however, it is unclear if or when these *Pd-l1*-expressing qMcSCs contribute to maintaining physiological pigmentation. Neither PD-1 nor PD-L1 KO mice are reported to have premature gray hair, and PD-L1 KO does not prematurely diminish the qMcSC pool (Figure 4B). This supports the idea that PD-L1 is not required by McSCs for normal hair repigmentation through adulthood. Rather, blocking PD-L1 *in vitro* demonstrates an intrinsic role for PD-L1 in restricting cell cycling. Independently, using single cell RNA sequencing we've also shown that *Pd-l1*-expressing qMcSCs *in vivo* express the highest level of cyclin dependent kinase inhibitors in comparison to all other qMcSCs.[40] This 'deep' quiescence may enhance the long-term maintenance of the PD-L1-expressing subpopulation of qMcSCs over time and explain why these qMcSCs appear to be resistant to age-associated McSC depletion (Figure 4F). In humans, gray hairs consistently retain a moderate number of melanocytes and McSCs, whereas white hairs are reported to have either small numbers of melanocytes and McSCs or are completely devoid of both.[20,74–77] Dramatic repigmentation of gray-haired patients after PD-1 or PD-L1 immunotherapy suggests that gray hairs may harbor inactive McSCs and demonstrates the capacity of these McSCs for reactivation in humans.[78,79] Based on the findings presented here, we predict that it is the PD-L1-expressing qMcSCs that are retained in non-pigmented and gray hairs, these cells are the target of anti-PD-L1 immunotherapy, and their presence is essential for the reversal of gray hair (Figure 7).

The role of PD-L1 has mostly been explored in the context of immune evasion by tumor cells and the pharmacological targeting of cellular immune checkpoints.[80–82] Localization of PD-L1 at the cell membrane allows PD-L1 to interact with PD-1 on T-cells, suppressing an immune response and providing cancer cells with immune privilege.[24,83] In combination with evidence supporting PD-L1 upregulation on cancer cells and its role in escape from the immune response,[84–86] the PD-1/PD-L1 axis has become a significant target for immunotherapy-based clinical cancer research, and treatments targeting this interaction have received regulatory approval for melanoma and subsequently for a variety of other cancer types.[87–89] Outside of oncology, physiological PD-L1 expression promotes immune tolerance in a variety of human and murine tissues, including the thymus, liver, lung, pancreas, eye, and placenta.[90,91] Hair follicle immune privilege has long been established, and protection of hair follicle stem cells during dormancy is attributed to the downregulation of MHC class I molecules that accompany hair follicle stem cell G_0.[92,93] However, until now, no studies have reported PD-L1 upregulation as an additional contributor to this hair privilege process, and no studies have asked whether McSCs that reside in hair follicles are also privileged. If PD-L1 also participates in G_0-mediated McSC immune evasion, this could explain the prevalence of vitiligo-like lesions in melanoma patients receiving anti-PD-1 or anti-PD-L1 immunotherapies due to common autoantigens between melanocytes and melanoma cells.[94,95]

Outside of immune privilege, the skin houses numerous immune cells that can express PD-1, whose functions are not limited to immunity. By engaging PD-L1, these PD-1-expressing cells could influence qMcSCs or vice versa. Macrophages and regulatory T cells can regulate hair follicle growth through direct and indirect interactions with hair follicle stem cells.[96–99] Depletion of either retards hair regrowth. If a similar interaction occurs between these immune cells and McSCs through PD-1/PD-L1 binding, this would provide an additional mechanism for coordinating cross-talk between immune and non-immune tissue populations. The relevance of these immune cells in McSC regeneration

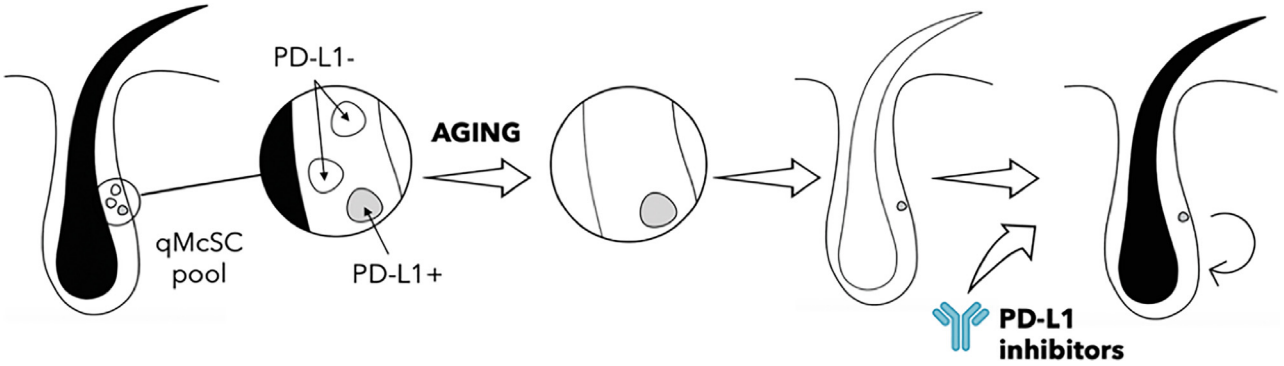

Figure 7. Predicted model of McSC aging and the potential of targeting PD-L1 for hair repigmentation

qMcSCs lacking PD-L1 expression are reduced over time through the canonical pathway for McSC loss and this leads to hair graying. qMcSCs that maintain PD-L1 expression are retained with age, which may be a feature of PD-L1-mediated quiescence reinforcement. Accordingly, we predict that PD-L1-expressing qMcSCs may not contribute to physiological hair repigmentation except under specific contexts. PD-1 or PD-L1 blockade may allow PD-L1-expressing qMcSCs to reenter the cell cycle and regenerate pigmentation in previously gray hairs.

or aging of the McSC pool could then be determined. In support of the idea that PD-L1 participates in functions beyond immune privilege within the skin, inhibiting PD-L1 during early entry into the anagen stage of the hair cycle accelerates the hair growth rate.[41] Recent studies also demonstrate that the PD-1/PD-L1 axis is not unidirectional and PD-L1 can transduce signals intrinsically that favor tumor progression. The intracellular domain of PD-L1 uses non-classical signaling motifs to protect against IFN-mediated apoptosis.[56,57,100] It appears that PD-L1 can also function independently of PD-1 engagement. For instance, PD-L1 is expressed by gut epithelium, is required for resistance to gut injury and inflammation, and PD-L1 presence is protective even in the absence of PD-1 expressing T cells in PD-1 knockout mice.[101] Signaling downstream of PD-L1, absent of PD-1 *in vitro,* can also regulate glycolysis of some tumor cell lines.[55]

Evidence from cancer research indicates an association between PD-L1 expression and cell cycle state. IFN-gamma is a popular cytokine used to stimulate membrane expression of PD-L1 in both tumorigenic and non-tumorigenic cells but also causes cell-cycle arrest.[102] However, in our *in vitro* G_0 model established above, we demonstrate that PD-L1 membrane expression is elevated in melb-a cells by cell-cycle arrest alone, independent of IFN-gamma signaling. In astrocytomas, membrane-associated PD-L1 expression was highly associated with non-proliferative, KI67-negative cells at the growing edge of tumors.[103] In this case, PD-L1 expression was independent of tumor stem cell-like properties but dependent on mitogenic availability, and thus the complex microenvironment observed within solid tumors may explain the heterogeneity in PD-L1 expression. Others have shown that CDK4 levels, an essential early-stage protein for re-entry into the cell cycle, can influence the abundance of membrane expression of PD-L1 in multiple tumor cell lines. By inhibiting CDK4 expression and causing cell-cycle arrest, degradation of PD-L1 is reduced and results in an increased PD-L1 expression.[104] Similarly, we demonstrate that the differential subcellular localization of PD-L1 may be intimately tied to G_0 status in qMcSCs. The increase in the proportion of membrane-associated PD-L1-expressing cells in aged qMcSCs is not predicted by gene expression; we show that *Pd-l1* is not differentially expressed when comparing the transcriptomes of adult and aged qMcSCs by RNA-Seq. We make a similar observation *in vitro*; increasing the duration of G_0 in melb-a cells does not alter *Pd-l1* expression at the transcript level but does lead to changes in PD-L1 protein localization and a higher proportion of cells exhibiting membrane-associated PD-L1 expression. This suggests that the post-translational regulation of PD-L1 may be an important aspect of the role of this protein during G_0. Using our *in vitro* quiescence model, we can test how the *Pd-l1* transcript and the PD-L1 protein are regulated at the transcriptional and posttranslational level in the context of quiescence induction and cell cycle reactivation. While the role of PD-L1 has been extensively evaluated in the context of cancer immunology, understanding how and why normal stem cells express and use PD-L1 physiologically offers a new perspective on how these pathways and cells are co-opted during tumorigenesis.

In summary, we interrogated the melanocyte lineage at the transcriptomic level to better understand how aging influences G_0 in McSCs. Aged qMcSCs appear more quiescent than their younger counterparts. Our *in vitro* and *in vivo* models of cellular quiescence show remarkable heterogeneity that includes differential expression of the immune privilege component *Pd-l1*. Functional assays *in vitro* demonstrate a novel role for PD-L1 in the regulation and maintenance of the quiescent state. Our characterization of PD-L1 *in vivo* shows that because PD-L1 negative qMcSCs are preferentially lost with age, the qMcSC pool shifts toward one with a greater proportion of PD-L1-expressing cells over time. Spatially directed cell-cell communication is indispensable for tissue development, cellular proliferation, and healthy aging.[105] While such characterization is beyond the scope of the present study, future single-cell whole-transcriptome profiling of McSCs within their microenvironment offers the opportunity to further define mechanisms (like PD-1 engagement) that could influence the regenerative potential of PD-L1-bearing qMcSCs. In addition, we anticipate that PD-L1 could be pharmacologically targeted for improved tissue regeneration within the pigment system or any other stem cell system that utilizes PD-L1 to regulate its quiescent state. In the last couple of years, there has been increased interest in PD-L1 in the context of aging,[106,107] and our work brings an additional perspective to that understanding.

Limitations of this study

The major focus of this paper is the novel association between PD-L1 and cellular quiescence and the potential of PD-L1 in reinforcing quiescence in the melanocyte cell lineage. Our gene expression data highlights additional transcriptional changes that occur as McSC transitions to quiescence and with age, and the contributions of those biological pathways to quiescence regulation during aging remain open for further study. The broader implications of this work will depend on the *in vivo* validation of PD-L1's role in quiescence regulation in McSCs and any other stem cell population that expresses PD-L1 during quiescence.

RESOURCE AVAILABILITY

Lead contact

Further information and requests for resources and reagents should be directed to and will be fulfilled by the lead contact, Dr. Melissa Harris (harrisml@uab.edu).

Materials availability

This study did not generate new unique reagents.

Data and code availability

- Data- RNA-seq data have been deposited at NCBI (GSE261101) and are publicly available as of the date of publication. DOIs are also listed in the key resources table.
- Code- This paper does not report original code.
- Any additional information required to reanalyze the data reported in this paper is available from the lead contact upon request.

ACKNOWLEDGMENTS

This research was supported by funding provided to MLH from the National Institute on Aging (R00AG047128), the UAB Faculty Development Grant Program, and start-up funds from the Department of Biology and College of Arts of Science at the University of Alabama at Birmingham. WPJ was supported by the National Human Genome Research Institute Intramural Research Program. Fellowship support was provided independently to JWP (UAB Blazer Fellowship). FVF is grateful for the support of Machine Learning and Multi-omics by the Bavaria California Technology Center, the Science Alliance on Precision Medicine and Cancer Prevention by the German Federal Foreign Office, and CA154887 by the National Cancer Institute. We acknowledge the NIH Intramural Sequencing Center for their high throughput sequencing services, and this includes Beatrice B. Barnabas, Gerard G. Bouffard, Shelise Y. Brooks, Holly Coleman, Lyudmila Dekhtyar, Xiaobin Guan, Joel Han, Shi-ling Ho, Richelle Legaspi, Quino L. Maduro, Catherine A. Masiello, Jennifer C. McDowell, Casandra Montemayor, James C. Mullikin, Morgan Park, Nancy L. Riebow, Karen Schandler, Brian Schmidt, Christina Sison, Raymond Smith, Sirintorn Stantripop, James W. Thomas, Pamela J. Thomas, Meghana Vemulapalli, and Alice C. Young. Additional thanks are given to Arlene Sharpe (Harvard Medical School, NIH grant P01AI056299) and members of the Sharpe Lab (Dr. Joon Seok Park and Cecilia Washburn) for providing tissue samples from PD-L1 WT and KO mice.

AUTHOR CONTRIBUTIONS

Conceptualization: JWP and MLH.

Data curation and formal analysis: JWP, KMV, MI, IJB, NP, AD, FVF, and MLH.

Funding acquisition: JWP and MLH.

Investigation: JWP, KMV, DW, IJB, NP, AD, MI, FVF, and MLH, methodology: JWP, KMV, MI, IJB, NP, NISC, and MLH.

Project administration: JWP and MLH.

Initial enrichment, gene network, and transcription factor analyses: JWP and FVF.

Final enrichment, gene network, and transcription factor analyses: JWP.

Resources: WJP and MLH, software: JWP.

Supervision: JWP and MLH.

Validation: JWP, KMV, IJB, MI, and MLH.

Visualization: JWP and MLH.

Writing – draft: JWP and MLH.

Writing – review and editing: JWP, FVF, and MLH.

Final manuscript approval: All authors.

DECLARATION OF INTERESTS

All authors declare no competing interests.

STAR★METHODS

Detailed methods are provided in the online version of this paper and include the following:

- KEY RESOURCES TABLE
- EXPERIMENTAL MODEL AND STUDY PARTICIPANT DETAILS
  - Animals
  - Cell lines
- METHOD DETAILS
  - Primary melanoblast and McSC enrichment and flow cytometry analysis
  - RNA isolation

- RNA-Seq and differential gene expression analysis
- qRT-PCR analysis
- Tissue and cell immunolabeling
- Hair counts
- Quiescence induction in melb-a cells
- PD-L1 blockade and *Pd-l1* knockdown in melb-a cells
- Flow cytometry of melb-a cells
- Protein quantification and western blotting

● QUANTIFICATION AND STATISTICAL ANALYSIS

SUPPLEMENTAL INFORMATION

Supplemental information can be found online at https://doi.org/10.1016/j.isci.2024.110908.

Received: April 24, 2024
Revised: July 17, 2024
Accepted: September 5, 2024
Published: September 12, 2024

REFERENCES

1. Ahmed, A.S.I., Sheng, M.H., Wasnik, S., Baylink, D.J., and Lau, K.-H.W. (2017). Effect of aging on stem cells. World J. Exp. Med. *7*, 1–10. https://doi.org/10.5493/wjem.v7.i1.1.
2. Oh, J., Lee, Y.D., and Wagers, A.J. (2014). Stem cell aging: mechanisms, regulators and therapeutic opportunities. Nat. Med. *20*, 870–880. https://doi.org/10.1038/nm.3651.
3. Cheung, H.-H., Pei, D., and Chan, W.-Y. (2015). Stem cell aging in adult progeria. Cell Regen. *4*, 6. https://doi.org/10.1186/s13619-015-0021-z.
4. Harris, M.L., Fufa, T.D., Palmer, J.W., Joshi, S.S., Larson, D.M., Incao, A., Gildea, D.E., Trivedi, N.S., Lee, A.N., Day, C.-P., et al. (2018). A direct link between MITF, innate immunity, and hair graying. PLoS Biol. *16*, e2003648. https://doi.org/10.1371/journal.pbio.2003648.
5. Inomata, K., Aoto, T., Binh, N.T., Okamoto, N., Tanimura, S., Wakayama, T., Iseki, S., Hara, E., Masunaga, T., Shimizu, H., and Nishimura, E.K. (2009). Genotoxic Stress Abrogates Renewal of Melanocyte Stem Cells by Triggering Their Differentiation. Cell *137*, 1088–1099. https://doi.org/10.1016/j.cell.2009.03.037.
6. Uno, M., and Nishida, E. (2016). Lifespan-regulating genes in C. elegans. NPJ Aging Mech. Dis. *2*, 16010. https://doi.org/10.1038/npjamd.2016.10.
7. Goodell, M.A., and Rando, T.A. (2015). Stem cells and healthy aging. Science *350*, 1199–1204. https://doi.org/10.1126/science.aab3388.
8. Tümpel, S., and Rudolph, K.L. (2019). Quiescence: Good and Bad of Stem Cell Aging. Trends Cell Biol. *29*, 672–685. https://doi.org/10.1016/j.tcb.2019.05.002.
9. Cho, I.J., Lui, P.P., Obajdin, J., Riccio, F., Stroukov, W., Willis, T.L., Spagnoli, F., and Watt, F.M. (2019). Mechanisms, Hallmarks, and Implications of Stem Cell Quiescence. Stem Cell Rep. *12*, 1190–1200. https://doi.org/10.1016/j.stemcr.2019.05.012.
10. Coller, H.A., Sang, L., and Roberts, J.M. (2006). A New Description of Cellular Quiescence. PLoS Biol. *4*, e83. https://doi.org/10.1371/journal.pbio.0040083.
11. Kwon, J.S., Everetts, N.J., Wang, X., Wang, W., Della Croce, K., Xing, J., and Yao, G. (2017). Controlling Depth of Cellular Quiescence by an Rb-E2F Network Switch. Cell Rep. *20*, 3223–3235. https://doi.org/10.1016/j.celrep.2017.09.007.
12. Urbán, N., and Cheung, T.H. (2021). Stem cell quiescence: the challenging path to activation. Development *148*, dev165084. https://doi.org/10.1242/dev.165084.
13. Cheung, T.H., and Rando, T.A. (2013). Molecular regulation of stem cell quiescence. Nat. Rev. Mol. Cell Biol. *14*, 329–340. https://doi.org/10.1038/nrm3591.
14. van Velthoven, C.T.J., and Rando, T.A. (2019). Stem Cell Quiescence: Dynamism, Restraint, and Cellular Idling. Cell Stem Cell *24*, 213–225. https://doi.org/10.1016/j.stem.2019.01.001.
15. Du, J., Chen, Y., Li, Q., Han, X., Cheng, C., Wang, Z., Danielpour, D., Dunwoodie, S.L., Bunting, K.D., and Yang, Y.-C. (2012). HIF-1α deletion partially rescues defects of hematopoietic stem cell quiescence caused by Cited2 deficiency. Blood *119*, 2789–2798. https://doi.org/10.1182/blood-2011-10-387902.
16. Mourikis, P., Sambasivan, R., Castel, D., Rocheteau, P., Bizzarro, V., and Tajbakhsh, S. (2012). A critical requirement for notch signaling in maintenance of the quiescent skeletal muscle stem cell state. Stem Cell. *30*, 243–252. https://doi.org/10.1002/stem.775.
17. Zhou, Y., Yan, X., Feng, X., Bu, J., Dong, Y., Lin, P., Hayashi, Y., Huang, R., Olsson, A., Andreassen, P.R., et al. (2018). Setd2 regulates quiescence and differentiation of adult hematopoietic stem cells by restricting RNA polymerase II elongation. Haematologica *103*, 1110–1123. https://doi.org/10.3324/haematol.2018.187708.
18. Slominski, A., Paus, R., Plonka, P., Chakraborty, A., Maurer, M., Pruski, D., and Lukiewicz, S. (1994). Melanogenesis During the Anagen-Catagen-Telogen Transformation of the Murine Hair Cycle. J. Invest. Dermatol. *102*, 862–869. https://doi.org/10.1111/1523-1747.ep12382606.
19. Slominski, A., Wortsman, J., Plonka, P.M., Schallreuter, K.U., Paus, R., and Tobin, D.J. (2005). Hair Follicle Pigmentation. J. Invest. Dermatol. *124*, 13–21. https://doi.org/10.1111/j.0022-202X.2004.23528.x.
20. Nishimura, E.K., Granter, S.R., and Fisher, D.E. (2005). Mechanisms of Hair Graying: Incomplete Melanocyte Stem Cell Maintenance in the Niche. Science *307*, 720–724. https://doi.org/10.1126/science.1099593.
21. Müller-Röver, S., Foitzik, K., Paus, R., Handjiski, B., van der Veen, C., Eichmüller, S., McKay, I.A., and Stenn, K.S. (2001). A Comprehensive Guide for the Accurate Classification of Murine Hair Follicles in Distinct Hair Cycle Stages. J. Invest. Dermatol. *117*, 3–15. https://doi.org/10.1046/j.0022-202x.2001.01377.x.
22. Diwakar, G., Zhang, D., Jiang, S., and Hornyak, T.J. (2008). Neurofibromin as a regulator of melanocyte development and differentiation. J. Cell Sci. *121*, 167–177. https://doi.org/10.1242/jcs.013912.
23. Dong, H., Zhu, G., Tamada, K., and Chen, L. (1999). B7-H1, a third member of the B7 family, co-stimulates T-cell proliferation and interleukin-10 secretion. Nat. Med. *5*, 1365–1369. https://doi.org/10.1038/70932.
24. Freeman, G.J., Long, A.J., Iwai, Y., Bourque, K., Chernova, T., Nishimura, H., Fitz, L.J., Malenkovich, N., Okazaki, T., Byrne, M.C., et al. (2000). Engagement of the PD-1 immunoinhibitory receptor by a novel B7 family member leads to negative regulation of lymphocyte activation. J. Exp. Med. *192*, 1027–1034. https://doi.org/10.1084/jem.192.7.1027.
25. Zhang, N., Zeng, Y., Du, W., Zhu, J., Shen, D., Liu, Z., and Huang, J.-A. (2016). The EGFR pathway is involved in the regulation of PD-L1 expression via the IL-6/JAK/STAT3 signaling pathway in EGFR-mutated non-small cell lung cancer. Int. J. Oncol. *49*, 1360–1368. https://doi.org/10.3892/ijo.2016.3632.
26. Casey, S.C., Tong, L., Li, Y., Do, R., Walz, S., Fitzgerald, K.N., Gouw, A.M., Baylot, V., Gütgemann, I., Eilers, M., and Felsher, D.W. (2016). MYC regulates the antitumor immune response through CD47 and PD-L1. Science *352*, 227–231. https://doi.org/10.1126/science.aac9935.
27. Garcia-Diaz, A., Shin, D.S., Moreno, B.H., Saco, J., Escuin-Ordinas, H., Rodriguez, G.A., Zaretsky, J.M., Sun, L., Hugo, W., Wang, X., et al. (2017). Interferon Receptor Signaling Pathways Regulating PD-L1 and PD-L2 Expression. Cell Rep. *19*, 1189–1201. https://doi.org/10.1016/j.celrep.2017.04.031.
28. Yi, M., Niu, M., Xu, L., Luo, S., and Wu, K. (2021). Regulation of PD-L1 expression in

the tumor microenvironment. J. Hematol. Oncol. *14*, 10. https://doi.org/10.1186/s13045-020-01027-5.

29. Rodgers, J.T., King, K.Y., Brett, J.O., Cromie, M.J., Charville, G.W., Maguire, K.K., Brunson, C., Mastey, N., Liu, L., Tsai, C.-R., et al. (2014). mTORC1 controls the adaptive transition of quiescent stem cells from G0 to GAlert. Nature *510*, 393–396. https://doi.org/10.1038/nature13255.
30. Sharifi, S., da Costa, H.F.R., and Bierhoff, H. (2020). The circuitry between ribosome biogenesis and translation in stem cell function and ageing. Mech. Ageing Dev. *189*, 111282. https://doi.org/10.1016/j.mad.2020.111282.
31. Basisty, N., Kale, A., Jeon, O.H., Kuehnemann, C., Payne, T., Rao, C., Holtz, A., Shah, S., Sharma, V., Ferrucci, L., et al. (2020). A proteomic atlas of senescence-associated secretomes for aging biomarker development. PLoS Biol. *18*, e3000599. https://doi.org/10.1371/journal.pbio.3000599.
32. Coppé, J.-P., Desprez, P.-Y., Krtolica, A., and Campisi, J. (2010). The Senescence-Associated Secretory Phenotype: The Dark Side of Tumor Suppression. Annu. Rev. Pathol. *5*, 99–118. https://doi.org/10.1146/annurev-pathol-121808-102144.
33. Tacutu, R., Thornton, D., Johnson, E., Budovsky, A., Barardo, D., Craig, T., Diana, E., Lehmann, G., Toren, D., Wang, J., et al. (2018). Human Ageing Genomic Resources: new and updated databases. Nucleic Acids Res. *46*, D1083–D1090. https://doi.org/10.1093/nar/gkx1042.
34. de Magalhães, J.P., Curado, J., and Church, G.M. (2009). Meta-analysis of age-related gene expression profiles identifies common signatures of aging. Bioinformatics *25*, 875–881. https://doi.org/10.1093/bioinformatics/btp073.
35. Johnson, S.C. (2018). Nutrient Sensing, Signaling and Ageing: The Role of IGF-1 and mTOR in Ageing and Age-Related Disease. Subcell. Biochem. *90*, 49–97. https://doi.org/10.1007/978-981-13-2835-0_3.
36. van Veelen, W., Korsse, S.E., van de Laar, L., and Peppelenbosch, M.P. (2011). The long and winding road to rational treatment of cancer associated with LKB1/AMPK/TSC/mTORC1 signaling. Oncogene *30*, 2289–2303. https://doi.org/10.1038/onc.2010.630.
37. Infarinato, N.R., Stewart, K.S., Yang, Y., Gomez, N.C., Pasolli, H.A., Hidalgo, L., Polak, L., Carroll, T.S., and Fuchs, E. (2020). BMP signaling: at the gate between activated melanocyte stem cells and differentiation. Genes Dev. *34*, 1713–1734. https://doi.org/10.1101/gad.340281.120.
38. Joshi, S.S., Tandukar, B., Pan, L., Huang, J.M., Livak, F., Smith, B.J., Hodges, T., Mahurkar, A.A., and Hornyak, T.J. (2019). CD34 defines melanocyte stem cell subpopulations with distinct regenerative properties. PLoS Genet. *15*, e1008034. https://doi.org/10.1371/journal.pgen.1008034.
39. Ueno, M., Aoto, T., Mohri, Y., Yokozeki, H., and Nishimura, E.K. (2014). Coupling of the radiosensitivity of melanocyte stem cells to their dormancy during the hair cycle. Pigment Cell Melanoma Res. *27*, 540–551. https://doi.org/10.1111/pcmr.12251.
40. Palmer, J.W., Kumar, N., An, L., White, A.C., Mukhtar, M.S., and Harris, M.L. (2024). Molecular heterogeneity of quiescent melanocyte stem cells revealed by single-cell RNA-sequencing. Pigment Cell Melanoma Res. *37*, 480–495. https://doi.org/10.1111/pcmr.13169.
41. Zhou, L., Wen, L., Sheng, Y., Lu, J., Hu, R., Wang, X., Lu, Z., and Yang, Q. (2021). The PD-1/PD-L1 pathway in murine hair cycle transition: a potential anagen phase regulator. Arch. Dermatol. Res. *313*, 751–758. https://doi.org/10.1007/s00403-020-02169-9.
42. Hirano, T., Honda, T., Kanameishi, S., Honda, Y., Egawa, G., Kitoh, A., Nakajima, S., Otsuka, A., Nomura, T., Dainichi, T., et al. (2021). PD-L1 on mast cells suppresses effector CD8+ T-cell activation in the skin in murine contact hypersensitivity. J. Allergy Clin. Immunol. *148*, 563–573.e7. https://doi.org/10.1016/j.jaci.2020.12.654.
43. Qin, W., Hu, L., Zhang, X., Jiang, S., Li, J., Zhang, Z., and Wang, X. (2019). The Diverse Function of PD-1/PD-L Pathway Beyond Cancer. Front. Immunol. *10*, 2298.
44. Neuwelt, A.J., Kimball, A.K., Johnson, A.M., Arnold, B.W., Bullock, B.L., Kaspar, R.E., Kleczko, E.K., Kwak, J.W., Wu, M.-H., Heasley, L.E., et al. (2020). Cancer cell-intrinsic expression of MHC II in lung cancer cell lines is actively restricted by MEK/ERK signaling and epigenetic mechanisms. J. Immunother. Cancer *8*, e000441. https://doi.org/10.1136/jitc-2019-000441.
45. Wu, B., Chiang, H.-C., Sun, X., Yuan, B., Mitra, P., Hu, Y., Curiel, T.J., and Li, R. (2020). Genetic ablation of adipocyte PD-L1 reduces tumor growth but accentuates obesity-associated inflammation. J. Immunother. Cancer *8*, e000964. https://doi.org/10.1136/jitc-2020-000964.
46. Joost, S., Annusver, K., Jacob, T., Sun, X., Dalessandri, T., Sivan, U., Sequeira, I., Sandberg, R., and Kasper, M. (2020). The Molecular Anatomy of Mouse Skin during Hair Growth and Rest. Cell Stem Cell *26*, 441–457.e7. https://doi.org/10.1016/j.stem.2020.01.012.
47. Sviderskaya, E.V., Wakeling, W.F., and Bennett, D.C. (1995). A cloned, immortal line of murine melanoblasts inducible to differentiate to melanocytes. Development *121*, 1547–1557.
48. Salic, A., and Mitchison, T.J. (2008). A chemical method for fast and sensitive detection of DNA synthesis *in vivo*. Proc. Natl. Acad. Sci. USA *105*, 2415–2420. https://doi.org/10.1073/pnas.0712168105.
49. Augenlicht, L.H., and Baserga, R. (1974). Changes in the G0 state of WI-38 fibroblasts at different times after confluence. Exp. Cell Res. *89*, 255–262. https://doi.org/10.1016/0014-4827(74)90789-7.
50. Gray, J.V., Petsko, G.A., Johnston, G.C., Ringe, D., Singer, R.A., and Werner-Washburne, M. (2004). "Sleeping Beauty": Quiescence in Saccharomyces cerevisiae. Microbiol. Mol. Biol. Rev. *68*, 187–206. https://doi.org/10.1128/MMBR.68.2.187-206.2004.
51. Lovén, J., Orlando, D.A., Sigova, A.A., Lin, C.Y., Rahl, P.B., Burge, C.B., Levens, D.L., Lee, T.I., and Young, R.A. (2012). Revisiting Global Gene Expression Analysis. Cell *151*, 476–482. https://doi.org/10.1016/j.cell.2012.10.012.
52. Rumman, M., Dhawan, J., and Kassem, M. (2015). Concise Review: Quiescence in Adult Stem Cells: Biological Significance and Relevance to Tissue Regeneration: ASC Quiescence: Role and Relevance to Tissue Regeneration. Stem Cell. *33*, 2903–2912. https://doi.org/10.1002/stem.2056.
53. Mak, S.-S., Moriyama, M., Nishioka, E., Osawa, M., and Nishikawa, S.-I. (2006). Indispensable role of Bcl2 in the development of the melanocyte stem cell. Dev. Biol. *291*, 144–153. https://doi.org/10.1016/j.ydbio.2005.12.025.
54. Peters, E.M.J., Maurer, M., Botchkarev, V.A., Jensen, K.d., Welker, P., Scott, G.A., and Paus, R. (2003). Kit Is Expressed by Epithelial Cells In Vivo. J. Invest. Dermatol. *121*, 976–984. https://doi.org/10.1046/j.1523-1747.2003.12478.x.
55. Chang, C.-H., Qiu, J., O'Sullivan, D., Buck, M.D., Noguchi, T., Curtis, J.D., Chen, Q., Gindin, M., Gubin, M.M., van der Windt, G.J.W., et al. (2015). Metabolic Competition in the Tumor Microenvironment Is a Driver of Cancer Progression. Cell *162*, 1229–1241. https://doi.org/10.1016/j.cell.2015.08.016.
56. Clark, C.A., Gupta, H.B., Sareddy, G., Pandeswara, S., Lao, S., Yuan, B., Drerup, J.M., Padron, A., Conejo-Garcia, J., Murthy, K., et al. (2016). Tumor-Intrinsic PD-L1 Signals Regulate Cell Growth, Pathogenesis, and Autophagy in Ovarian Cancer and Melanoma. Cancer Res. *76*, 6964–6974. https://doi.org/10.1158/0008-5472.CAN-16-0258.
57. Gato-Cañas, M., Zuazo, M., Arasanz, H., Ibañez-Vea, M., Lorenzo, L., Fernandez-Hinojal, G., Vera, R., Smerdou, C., Martisova, E., Arozarena, I., et al. (2017). PDL1 Signals through Conserved Sequence Motifs to Overcome Interferon-Mediated Cytotoxicity. Cell Rep. *20*, 1818–1829. https://doi.org/10.1016/j.celrep.2017.07.075.
58. Yale, K., Juhasz, M., and Atanaskova Mesinkovska, N. (2020). Medication-Induced Repigmentation of Gray Hair: A Systematic Review. Skin Appendage Disord. *6*, 1–10. https://doi.org/10.1159/000504414.
59. Chen, C.-C., Murray, P.J., Jiang, T.X., Plikus, M.V., Chang, Y.-T., Lee, O.K., Widelitz, R.B., and Chuong, C.-M. (2014). Regenerative Hair Waves in Aging Mice and Extra-Follicular Modulators Follistatin, Dkk1, and Sfrp4. J. Invest. Dermatol. *134*, 2086–2096. https://doi.org/10.1038/jid.2014.139.
60. Cho, A.-R., Kim, J.Y., Munkhbayer, S., Shin, C.-Y., and Kwon, O. (2016). p21 upregulation in hair follicle stem cells is associated with telogen retention in aged mice. Exp. Dermatol. *25*, 76–78. https://doi.org/10.1111/exd.12862.
61. Keyes, B.E., Segal, J.P., Heller, E., Lien, W.-H., Chang, C.-Y., Guo, X., Oristian, D.S., Zheng, D., and Fuchs, E. (2013). Nfatc1 orchestrates aging in hair follicle stem cells. Proc. Natl. Acad. Sci. USA *110*, E4950–E4959. https://doi.org/10.1073/pnas.1320301110.
62. Kalamakis, G., Brüne, D., Ravichandran, S., Bolz, J., Fan, W., Ziebell, F., Stiehl, T., Catalá-Martinez, F., Kupke, J., Zhao, S., et al. (2019). Quiescence Modulates Stem Cell Maintenance and Regenerative Capacity in the Aging Brain. Cell *176*, 1407–1419.e14. https://doi.org/10.1016/j.cell.2019.01.040.
63. Leeman, D.S., Hebestreit, K., Ruetz, T., Webb, A.E., McKay, A., Pollina, E.A., Dulken, B.W., Zhao, X., Yeo, R.W., Ho, T.T., et al. (2018). Lysosome activation clears aggregates and enhances quiescent neural stem cell activation during aging. Science *359*, 1277–1283. https://doi.org/10.1126/science.aag3048.

64. Janzen, V., Forkert, R., Fleming, H.E., Saito, Y., Waring, M.T., Dombkowski, D.M., Cheng, T., DePinho, R.A., Sharpless, N.E., and Scadden, D.T. (2006). Stem-cell ageing modified by the cyclin-dependent kinase inhibitor p16INK4a. Nature *443*, 421–426. https://doi.org/10.1038/nature05159.
65. Krishnamurthy, J., Ramsey, M.R., Ligon, K.L., Torrice, C., Koh, A., Bonner-Weir, S., and Sharpless, N.E. (2006). p16 INK4a induces an age-dependent decline in islet regenerative potential. Nature *443*, 453–457. https://doi.org/10.1038/nature05092.
66. Adelman, R.C., Stein, G., Roth, G.S., and Englander, D. (1972). Age-dependent regulation of mammalian DNA synthesis and cell proliferation In vivo. Mech. Ageing Dev. *1*, 49–59. https://doi.org/10.1016/0047-6374(72)90052-8.
67. Bucher, N.L.R., and Swaffield, M.N. (1964). The Rate of Incorporation of Labeled Thymidine into the Deoxyribonucleic Acid of Regenerating Rat Liver in Relation to the Amount of Liver Excised. Cancer Res. *24*, 1611–1625.
68. Bucher, N.L., Swaffield, M.N., and Ditroia, J.F. (1964). The Influence Of Age Upon The Incorporation Of Thymidine-2-C14 into the DNA of regenerating rat liver. Cancer Res. *24*, 509–512.
69. Liu, L., Cheung, T.H., Charville, G.W., Hurgo, B.M.C., Leavitt, T., Shih, J., Brunet, A., and Rando, T.A. (2013). Chromatin Modifications as Determinants of Muscle Stem Cell Quiescence and Chronological Aging. Cell Rep. *4*, 189–204. https://doi.org/10.1016/j.celrep.2013.05.043.
70. Conboy, I.M., Conboy, M.J., Smythe, G.M., and Rando, T.A. (2003). Notch-Mediated Restoration of Regenerative Potential to Aged Muscle. Science *302*, 1575–1577. https://doi.org/10.1126/science.1087573.
71. Iakova, P., Awad, S.S., and Timchenko, N.A. (2003). Aging Reduces Proliferative Capacities of Liver by Switching Pathways of C/EBPα Growth Arrest. Cell *113*, 495–506. https://doi.org/10.1016/S0092-8674(03)00318-0.
72. Katsimpardi, L., Litterman, N.K., Schein, P.A., Miller, C.M., Loffredo, F.S., Wojtkiewicz, G.R., Chen, J.W., Lee, R.T., Wagers, A.J., and Rubin, L.L. (2014). Vascular and Neurogenic Rejuvenation of the Aging Mouse Brain by Young Systemic Factors. Science *344*, 630–634. https://doi.org/10.1126/science.1251141.
73. Sun, Q., Lee, W., Hu, H., Ogawa, T., De Leon, S., Katehis, I., Lim, C.H., Takeo, M., Cammer, M., Taketo, M.M., et al. (2023). Dedifferentiation maintains melanocyte stem cells in a dynamic niche. Nature *616*, 774–782. https://doi.org/10.1038/s41586-023-05960-6.
74. Arck, P.C., Overall, R., Spatz, K., Liezman, C., Handjiski, B., Klapp, B.F., Birch-Machin, M.A., and Peters, E.M.J. (2006). Towards a "free radical theory of graying": melanocyte apoptosis in the aging human hair follicle is an indicator of oxidative stress induced tissue damage. FASEB J. *20*, 1567–1569. https://doi.org/10.1096/fj.05-4039fje.
75. Commo, S., Gaillard, O., and Bernard, B.A. (2004). Human hair greying is linked to a specific depletion of hair follicle melanocytes affecting both the bulb and the outer root sheath. Br. J. Dermatol. *150*, 435–443. https://doi.org/10.1046/j.1365-2133.2004.05787.x.
76. Horikawa, T., Norris, D.A., Johnson, T.W., Zekman, T., Dunscomb, N., Bennion, S.D., Jackson, R.L., and Morelli, J.G. (1996). DOPA-Negative Melanocytes in the Outer Root Sheath of Human Hair Follicles Express Premelanosomal Antigens But Not a Melanosomal Antigen or the Melanosome-Associated Glycoproteins Tyrosinase, TRP-1, and TRP-2. J. Invest. Dermatol. *106*, 28–35. https://doi.org/10.1111/1523-1747.ep12326989.
77. Takada, K., Sugiyama, K., Yamamoto, I., Óba, K., and Takeuchi, T. (1992). Presence of Amelanotic Melanocytes Within the Outer Root Sheath in Senile White Hair. J. Invest. Dermatol. *99*, 629–633. https://doi.org/10.1111/1523-1747.ep12668031.
78. Manson, G., Marabelle, A., and Houot, R. (2018). Hair Repigmentation With Anti–PD-1 and Anti–PD-L1 Immunotherapy: A Novel Hypothesis. JAMA Dermatol. *154*, 113. https://doi.org/10.1001/jamadermatol.2017.4421.
79. Rivera, N., Boada, A., Bielsa, M.I., Fernández-Figueras, M.T., Carcereny, E., Moran, M.T., and Ferrándiz, C. (2017). Hair Repigmentation During Immunotherapy Treatment With an Anti–Programmed Cell Death 1 and Anti–Programmed Cell Death Ligand 1 Agent for Lung Cancer. JAMA Dermatol. *153*, 1162–1165. https://doi.org/10.1001/jamadermatol.2017.2106.
80. McDermott, D.F., Sosman, J.A., Sznol, M., Massard, C., Gordon, M.S., Hamid, O., Powderly, J.D., Infante, J.R., Fassò, M., Wang, Y.V., et al. (2016). Atezolizumab, an Anti-Programmed Death-Ligand 1 Antibody, in Metastatic Renal Cell Carcinoma: Long-Term Safety, Clinical Activity, and Immune Correlates From a Phase Ia Study. J. Clin. Oncol. *34*, 833–842. https://doi.org/10.1200/JCO.2015.63.7421.
81. Socinski, M.A., Jotte, R.M., Cappuzzo, F., Orlandi, F., Stroyakovskiy, D., Nogami, N., Rodríguez-Abreu, D., Moro-Sibilot, D., Thomas, C.A., Barlesi, F., et al. (2018). Atezolizumab for First-Line Treatment of Metastatic Nonsquamous NSCLC. N. Engl. J. Med. *378*, 2288–2301. https://doi.org/10.1056/NEJMoa1716948.
82. Antonia, S.J., Balmanoukian, A., Brahmer, J., Ou, S.-H.I., Hellmann, M.D., Kim, S.-W., Ahn, M.-J., Kim, D.-W., Gutierrez, M., Liu, S.V., et al. (2019). Clinical Activity, Tolerability, and Long-Term Follow-Up of Durvalumab in Patients With Advanced NSCLC. J. Thorac. Oncol. *14*, 1794–1806. https://doi.org/10.1016/j.jtho.2019.06.010.
83. Carter, L., Fouser, L.A., Jussif, J., Fitz, L., Deng, B., Wood, C.R., Collins, M., Honjo, T., Freeman, G.J., and Carreno, B.M. (2002). PD-1:PD-L inhibitory pathway affects both CD4(+) and CD8(+) T cells and is overcome by IL-2. Eur. J. Immunol. *32*, 634–643. https://doi.org/10.1002/1521-4141(200203)32:3<634::AID-IMMU634>3.0.CO;2-9.
84. Iwai, Y., Ishida, M., Tanaka, Y., Okazaki, T., Honjo, T., and Minato, N. (2002). Involvement of PD-L1 on tumor cells in the escape from host immune system and tumor immunotherapy by PD-L1 blockade. Proc. Natl. Acad. Sci. USA *99*, 12293–12297. https://doi.org/10.1073/pnas.192461099.
85. Meng, Y., Liang, H., Hu, J., Liu, S., Hao, X., Wong, M.S.K., Li, X., and Hu, L. (2018). PD-L1 Expression Correlates With Tumor Infiltrating Lymphocytes And Response To Neoadjuvant Chemotherapy In Cervical Cancer. J. Cancer *9*, 2938–2945. https://doi.org/10.7150/jca.22532.
86. Zhang, L., Gajewski, T.F., and Kline, J. (2009). PD-1/PD-L1 interactions inhibit antitumor immune responses in a murine acute myeloid leukemia model. Blood *114*, 1545–1552. https://doi.org/10.1182/blood-2009-03-206672.
87. Raedler, L.A. (2015). Keytruda (Pembrolizumab): First PD-1 Inhibitor Approved for Previously Treated Unresectable or Metastatic Melanoma. Am. Health Drug Benefits *8*, 96–100.
88. Gong, J., Chehrazi-Raffle, A., Reddi, S., and Salgia, R. (2018). Development of PD-1 and PD-L1 inhibitors as a form of cancer immunotherapy: a comprehensive review of registration trials and future considerations. J. Immunother. Cancer *6*, 8. https://doi.org/10.1186/s40425-018-0316-z.
89. Akinleye, A., and Rasool, Z. (2019). Immune checkpoint inhibitors of PD-L1 as cancer therapeutics. J. Hematol. Oncol. *12*, 92. https://doi.org/10.1186/s13045-019-0779-5.
90. Bardhan, K., Anagnostou, T., and Boussiotis, V.A. (2016). The PD1:PD-L1/2 Pathway from Discovery to Clinical Implementation. Front. Immunol. *7*, 550. https://doi.org/10.3389/fimmu.2016.00550.
91. Keir, M.E., Butte, M.J., Freeman, G.J., and Sharpe, A.H. (2008). PD-1 and Its Ligands in Tolerance and Immunity. Annu. Rev. Immunol. *26*, 677–704. https://doi.org/10.1146/annurev.immunol.26.021607.090331.
92. Agudo, J., Park, E.S., Rose, S.A., Alibo, E., Sweeney, R., Dhainaut, M., Kobayashi, K.S., Sachidanandam, R., Baccarini, A., Merad, M., and Brown, B.D. (2018). Quiescent Tissue Stem Cells Evade Immune Surveillance. Immunity *48*, 271–285.e5. https://doi.org/10.1016/j.immuni.2018.02.001.
93. Paus, R., Ito, N., Takigawa, M., and Ito, T. (2003). The Hair Follicle and Immune Privilege. J. Investig. Dermatol. Symp. Proc. *8*, 188–194. https://doi.org/10.1046/j.1087-0024.2003.00807.x.
94. Mineiro Dos Santos Garrett, N.F., Carvalho da Costa, A.C., Barros Ferreira, E., Damiani, G., Diniz Dos Reis, P.E., and Inocêncio Vasques, C. (2021). Prevalence of dermatological toxicities in patients with melanoma undergoing immunotherapy: Systematic review and meta-analysis. PLoS One *16*, e0255716. https://doi.org/10.1371/journal.pone.0255716.
95. Guida, M., Strippoli, S., Maule, M., Quaglino, P., Ramondetta, A., Chiaron Sileni, V., Antonini Cappellini, G., Queirolo, P., Ridolfi, L., Del Vecchio, M., et al. (2021). Immune checkpoint inhibitor associated vitiligo and its impact on survival in patients with metastatic melanoma: an Italian Melanoma Intergroup study. ESMO Open *6*, 100064. https://doi.org/10.1016/j.esmoop.2021.100064.
96. Ali, N., Zirak, B., Rodriguez, R.S., Pauli, M.L., Truong, H.-A., Lai, K., Ahn, R., Corbin, K., Lowe, M.M., Scharschmidt, T.C., et al. (2017). Regulatory T cells in Skin Facilitate Epithelial Stem Cell Differentiation. Cell *169*, 1119–1129.e11. https://doi.org/10.1016/j.cell.2017.05.002.
97. Castellana, D., Paus, R., and Perez-Moreno, M. (2014). Macrophages Contribute to the Cyclic Activation of Adult Hair Follicle Stem Cells. PLoS Biol. *12*, e1002002. https://doi.org/10.1371/journal.pbio.1002002.

98. Chen, C.-C., Wang, L., Plikus, M.V., Jiang, T.X., Murray, P.J., Ramos, R., Guerrero-Juarez, C.F., Hughes, M.W., Lee, O.K., Shi, S., et al. (2015). Organ-Level Quorum Sensing Directs Regeneration in Hair Stem Cell Populations. Cell *161*, 277–290. https://doi.org/10.1016/j.cell.2015.02.016.

99. Osaka, N., Takahashi, T., Murakami, S., Matsuzawa, A., Noguchi, T., Fujiwara, T., Aburatani, H., Moriyama, K., Takeda, K., and Ichijo, H. (2007). ASK1-dependent recruitment and activation of macrophages induce hair growth in skin wounds. J. Cell Biol. *176*, 903–909. https://doi.org/10.1083/jcb.200611015.

100. Azuma, T., Yao, S., Zhu, G., Flies, A.S., Flies, S.J., and Chen, L. (2008). B7-H1 is a ubiquitous antiapoptotic receptor on cancer cells. Blood *111*, 3635–3643. https://doi.org/10.1182/blood-2007-11-123141.

101. Scandiuzzi, L., Ghosh, K., Hofmeyer, K.A., Abadi, Y.M., Lázár-Molnár, E., Lin, E.Y., Liu, Q., Jeon, H., Almo, S.C., Chen, L., et al. (2014). Tissue-Expressed B7-H1 Critically Controls Intestinal Inflammation. Cell Rep. *6*, 625–632. https://doi.org/10.1016/j.celrep.2014.01.020.

102. Chin, Y.E., Kitagawa, M., Su, W.C., You, Z.-H., Iwamoto, Y., and Fu, X.-Y. (1996). Cell Growth Arrest and Induction of Cyclin-Dependent Kinase Inhibitor p21WAF1/CIP1 Mediated by STAT1. Science *272*, 719–722. https://doi.org/10.1126/science.272.5262.719.

103. Yao, Y., Tao, R., Wang, X., Wang, Y., Mao, Y., and Zhou, L.F. (2009). B7-H1 is correlated with malignancy-grade gliomas but is not expressed exclusively on tumor stem-like cells. Neuro Oncol. *11*, 757–766. https://doi.org/10.1215/15228517-2009-014.

104. Zhang, J., Bu, X., Wang, H., Zhu, Y., Geng, Y., Nihira, N.T., Tan, Y., Ci, Y., Wu, F., Dai, X., et al. (2018). Cyclin D–CDK4 kinase destabilizes PD-L1 via cullin 3–SPOP to control cancer immune surveillance. Nature *553*, 91–95. https://doi.org/10.1038/nature25015.

105. Filipp, F.V. (2023). Spatial Cancer Systems Biology Resolves Heterotypic Interactions and Identifies Disruption of Spatial Hierarchy as a Pathological Driver Event. J. Invest. Dermatol. *143*, 1342–1347. https://doi.org/10.1016/j.jid.2023.02.006.

106. Onorati, A., Havas, A.P., Lin, B., Rajagopal, J., Sen, P., Adams, P.D., and Dou, Z. (2022). Upregulation of PD-L1 in Senescence and Aging. Mol. Cell Biol. *42*, e00171-22. https://doi.org/10.1128/mcb.00171-22.

107. Wang, T.-W., Johmura, Y., Suzuki, N., Omori, S., Migita, T., Yamaguchi, K., Hatakeyama, S., Yamazaki, S., Shimizu, E., Imoto, S., et al. (2022). Blocking PD-L1–PD-1 improves senescence surveillance and ageing phenotypes. Nature *611*, 358–364. https://doi.org/10.1038/s41586-022-05388-4.

108. Sviderskaya, E.V., Hill, S.P., Evans-Whipp, T.J., Chin, L., Orlow, S.J., Easty, D.J., Cheong, S.C., Beach, D., DePinho, R.A., and Bennett, D.C. (2002). p16Ink4a in melanocyte senescence and differentiation. J. Natl. Cancer Inst. *94*, 446–454.

109. Peters, E.M.J., Tobin, D.J., Botchkareva, N., Maurer, M., and Paus, R. (2002). Migration of Melanoblasts into the Developing Murine Hair Follicle Is Accompanied by Transient c-Kit Expression. J. Histochem. Cytochem. *50*, 751–766. https://doi.org/10.1177/002215540205000602.

110. Nishimura, E.K., Jordan, S.A., Oshima, H., Yoshida, H., Osawa, M., Moriyama, M., Jackson, I.J., Barrandon, Y., Miyachi, Y., and Nishikawa, S.-I. (2002). Dominant role of the niche in melanocyte stem-cell fate determination. Nature *416*, 854–860. https://doi.org/10.1038/416854a.

111. Szklarczyk, D., Gable, A.L., Lyon, D., Junge, A., Wyder, S., Huerta-Cepas, J., Simonovic, M., Doncheva, N.T., Morris, J.H., Bork, P., et al. (2019). STRING v11: protein–protein association networks with increased coverage, supporting functional discovery in genome-wide experimental datasets. Nucleic Acids Res. *47*, D607–D613. https://doi.org/10.1093/nar/gky1131.

112. Shannon, P., Markiel, A., Ozier, O., Baliga, N.S., Wang, J.T., Ramage, D., Amin, N., Schwikowski, B., and Ideker, T. (2003). Cytoscape: a software environment for integrated models of biomolecular interaction networks. Genome Res. *13*, 2498–2504. https://doi.org/10.1101/gr.1239303.

113. Su, G., Morris, J.H., Demchak, B., and Bader, G.D. (2014). Biological network exploration with Cytoscape 3. Curr. Protoc. Bioinformatics *47*, 8.13.1–8.13.24. https://doi.org/10.1002/0471250953.bi0813s47.

114. Chen, E.Y., Tan, C.M., Kou, Y., Duan, Q., Wang, Z., Meirelles, G.V., Clark, N.R., and Ma'ayan, A. (2013). Enrichr: interactive and collaborative HTML5 gene list enrichment analysis tool. BMC Bioinf. *14*, 128. https://doi.org/10.1186/1471-2105-14-128.

115. Anderson, Z.T., Palmer, J.W., Idris, M.I., Villavicencio, K.M., Le, G., Cowart, J., Weinstein, D.E., and Harris, M.L. (2021). Topical RT1640 treatment effectively reverses gray hair and stem cell loss in a mouse model of radiation-induced canities. Pigment Cell Melanoma Res. *34*, 89–100. https://doi.org/10.1111/pcmr.12913.

STAR★METHODS

KEY RESOURCES TABLE

REAGENT or RESOURCE	SOURCE	IDENTIFIER
Antibodies		
KIT-PE-CY7 (CD117)	BD Pharmingen	RRID: AB_469644
anti-CD45.2-FITC	BD Biosciences	RRID: AB_395041
anti-PD-L1-PE	Invitrogen	RRID: AB_466089
anti-PD-L1	Thermo Fisher Scientific	RRID: AB_467781
anti-DCT	Santa Cruz Biotechnology	RRID: AB_793582
anti-MKI67	Abcam	RRID: AB_302459
IgG2b isotype control antibody	BioXCell	RRID: AB_1107780
anti-PD-L1	BioXCell	RRID: AB_10949073
anti-PCNA	Abcam	RRID: AB_303394
anti-β-ACTIN-HRP	Proteintech	RRID: AB_2819183
Biological samples		
C57BL6-*Cd274*^{tm2Shr} mouse tissues	Dr. Arlene Sharpe, Harvard Medical School	–
Chemicals, peptides, and recombinant proteins		
Liberase TL	Roche	0540102001
Critical commercial assays		
EdU Click-iT assay	Thermo Fisher Scientific	C10632
Deposited data		
RNA-sequencing	Deposited at NCBI GEO	GSE261101
Experimental models: Cell lines		
Melb-a immortalized melanoblast cell line	Wellcome Trust Functional Genomics Cell Bank	RRID: CVCL_C693
RAW264.7 immortalized macrophage cell line	Dr. Andrzej Slominski	–
Experimental models: Organisms/strains		
C57BL/6J mice	The Jackson Laboratory	RRID: IMSR_JAX:000664
Aged C57BL/6 mice	NIA Aged Rodent Colony	RRID:SCR_007317)
Oligonucleotides		
Taqman Assay Cd274	Thermo Fisher Scientific	Mm03048248_m1
Taqman Assay *Cdk2*	Thermo Fisher Scientific	Mm00443947_m1
Taqman Assay *Cdk4*	Thermo Fisher Scientific	Mm00726334_s1
Taqman Assay *Cdkn1a*	Thermo Fisher Scientific	Mm01303209_m1
Taqman Assay *Cdkn1b*	Thermo Fisher Scientific	Mm00438168_m1
Taqman Assay *Cdkn2a*	Thermo Fisher Scientific	Mm00494449_m1
Taqman Assay *Mki67*	Thermo Fisher Scientific	Mm01278617_m1
Taqman Assay *Pdcd1*	Thermo Fisher Scientific	Mm01285676_m1
Taqman Assay *Gapdh*	Thermo Fisher Scientific	4352932E
Taqman Assay *Actb*	Thermo Fisher Scientific	Mm00607939_s1
Anti-Pd-l1 (Cd274) siRNA	Integrated DNA Technology	mm.Ri.Cd274.13.1
Software and algorithms		
Samtools	Babraham Bioinformatics	RRID:SCR_014583
Bam2fastq	Hudson Alpha	https://github.com/jts/bam2fastq

(*Continued on next page*)

Continued

REAGENT or RESOURCE	SOURCE	IDENTIFIER
FastQC	Babraham Bioinformatics	RRID:SCR_014583
Trimmomatic	Babraham Bioinformatics	RRID:SCR_011848
STAR	Alexander Dobin et al.	RRID:SCR_015899
DESeq2	Michael Love et al.	RRID:SCR_015687
R	R Core Team	https://www.R-project.org/

EXPERIMENTAL MODEL AND STUDY PARTICIPANT DETAILS

Animals

Animals used for RNA-Seq and hair color analysis were housed at the animal facilities at NHGRI. 8-week-old C57BL/6J wildtype females and pups (P0.5) were derived from in-house mating of C57BL/6J mice obtained from The Jackson Laboratory (RRID: IMSR_JAX:000664). 24-month-old C57BL/6 wild-type female mice were obtained through the NIA Aged Rodent Colony at Charles River Laboratories (RRID:SCR_007317) at 21 months old and allowed to age to 24 months within the same facility as the adult 8-week-old and P0.5 pups to which they were compared.

Animals used for flow cytometry were housed at the animal facilities at UAB. 8-week-old female C57BL/6J wildtype mice (RRID: IMSR_JAX:000664) used for the flow cytometry data presented in Figures 4D and 4E were obtained from JAX. 10-week-old and 24-month-old C57BL/6 wild-type mice used for the flow cytometry data presented in Figure 4F were obtained from the NIA Aged Rodent Colony (Charles River Laboratories, RRID:SCR_007317). All animals transferred to UAB were acclimatized within the mouse facilities for at least one week prior to experimentation.

Fixed skins from PD-L1 WT and KO mice (C57BL6-*Cd274*^{tm2Shn}) were obtained from Dr. Arlene Sharpe (Harvard Medical School).

Animal care and experimental animal procedures were performed in accordance with the guidelines set forth by the Public Health Service and Office of Laboratory Animal Welfare as designated by the Institutional Animal Care and Use Committee associated with UAB and NHGRI. This research is associated with the following animal protocols: UAB 20382 (to MLH), NHGRI G-94-7 (to WJP).

Cell lines

Melb-a cells (RRID: CVCL_C693) were obtained from the Wellcome Trust Functional Genomics Cell Bank.[108] For general cell growth and passaging, cells were incubated at 37°C and 10% CO2 in "full media" consisting of a RPMI 1640 with L-Glutamine (RPMI, Gibco, 11875-093) supplemented with 10% heat-inactivated fetal bovine serum (hi-FBS, Gibco, 16140-071), 100U/mL Penicillin/100ug/mL Streptomycin (pen/strep, Gibco, 15140-122), 20ng/mL SCF (Thermo Fisher Scientific PMC2111) and 0.6ng/mL bFGF (Stemgent 03-0002). This line is authenticated routinely using the following approaches (as recommended by ATCC): 1) check cell expected morphology and gene expression (shape, pigmentation, melanocyte differentiation genes); 2) check proliferation rate to assess abnormalities associated with passaging; 3) perform melanocyte marker analysis via immunolabeling to assess for cell type purity.

The murine macrophage line RAW264.7 was obtained from Dr. Andrzej Slominski (gift), and cultured using DMEM supplemented with 10% FBS and 1x antibiotic-antimycotic (Thermofisher, cat no 15240062). For cells utilized for RNA, cells were seeded at a density of 1x10^6 cells in a 6-well dish and allowed 48 hours of incubation before being harvested in 1 mL of Trizol reagent (Thermofisher, cat no 15596026).

METHOD DETAILS

Primary melanoblast and McSC enrichment and flow cytometry analysis

Dermis from postnatal day 0.5, 8-10-week, and 24-month mouse body skin was dissociated and processed using FACS to obtain enriched populations of melanoblasts, adult and aged qMcSCs, respectively.[4] Cells of the melanocyte lineage were identified by their surface expression of the receptor KIT. Melanoblasts in the P0.5 dermis are located within developing hair follicles.[109] Enrichment for qMcSCs at both the adult and aged timepoints was achieved by isolating KIT+CD45- cells from mouse skin whose hair was in the telogen stage of the hair cycle. McSC enrichment at telogen is dependent on the fact that telogen hairs contain only McSCs and do not contain differentiated melanocytes.[110] The telogen stage of the hair cycle was confirmed by the pinkness of the skin.[21] Female mice were used for all melanoblast and McSC enrichments as it is technically challenging to dissociate and obtain cells of high quality from male skin.

In brief, trunk skin was obtained and the subcutis removed by gentle scraping with curved forceps. The remaining skin was incubated at 37°C in 0.25% Trypsin-EDTA (Gibco 25200-056) for 20 minutes and then the dermis was separated from the epidermis by gentle scraping with curved forceps. The resulting dermis was minced using curved surgical scissors and dissociated by enzymatic treatment with 0.3mg/mL Liberase TL (Roche 0540102001) for 45-50 minutes at 37°C. Enzymatic digestion was stopped using a solution of DMEM containing 20% FBS and 0.5 mg/ml Dnase (Sigma DN-25). The dermis was physically disrupted by forcefully passing the dermal cell solution through a 70 μM Filcon filter (070-67S) fitted to a 50mL luerlock syringe (Soft-Ject, 8300006682). Cells were washed using a freshly prepared FACS wash solution consisting of 1X DPBS, 5% FBS, 25mM HEPES, and 2mM EDTA before being pelleted at 350 x g for 7 min at 4°C. Cells were resuspended and stained using cell surface antibody markers preconjugated to a fluorophore: KIT-PE-CY7 (CD117, BD Pharmingen 25-1171-82,

RRID: AB_469644), CD45.2-FITC (BD Biosciences 553772, RRID:AB_395041) and PD-L1-PE (Invitrogen 12-5982-82, RRID:AB_466089). Fluorescence was assessed by flow cytometry using an Biorad S3e cell sorter equipped with 488/561 lasers or a FACSAria (Becton Dickinson). Analysis of flow cytometry data was performed using FlowJo software (V10.6.0, RRID:SCR_008520). For sorting of cells on the Biorad S3e cell sorter, melanoblasts and melanocyte stem cells were positively selected by gating on the KIT+/CD45.2- cell population while mast cells were negatively selected by removing double-positive KIT+/CD45.2+ cells.

RNA isolation

Cellular RNA was purified using the Directzol RNA Miniprep Kit (Zymo R2062). For RNA-Seq, RNA was treated with 0.8U/µl RNase inhibitor. RNA was quantified using a Qubit fluorometer. RNA quality was determined by Bioanalyzer and RNA samples with a RIN score >8.5 were used for sequencing. For qPCR, RNA was isolated similarly but quantified using an Epoch spectrophotometer (Biotek).

RNA-Seq and differential gene expression analysis

McSCs from 3-4 animals were pooled to generate enough RNA to serve as one biological replicate. Amplified cDNA was created from 20 ng total RNA using the Ovation RNA-Seq System V2 (Tecan Genomics). The cDNA was fragmented using a Covaris E210 before proceeding to library construction with 1000ng cDNA using TruSeq RNA Sample Prep Kit, version 2 (Illumina) using 10 PCR cycles. Libraries were pooled in equimolar ratio and sequenced together on a HiSeq 2500 with version 3 flow cells and sequencing reagents. At least 60 million 126-base read pairs were generated for each library. Data were processed using RTA 1.18.64 and CASAVA 1.8.2. RNA-Seq reads that passed the Illumina platform quality check were used for downstream analyses.

Bam files were assessed for low-quality reads and removed before converting to fastq file format using samtools (v1.9, RRID:SCR_014583) and Bam2fastq (v1.1.0) software. Read quality was assessed using FastQC (v0.11.8, RRID:SCR_014583) and trimming was performed using Trimmomatic (v0.36, RRID:SCR_011848). Reads with a Phred quality score of 30 were pairwise removed and the remaining paired reads were trimmed to an average length of 90 base pairs. Reads were aligned to the Ensembl (RRID:SCR_002344) mouse mm10 reference genome with the STAR (v2.5.2, RRID:SCR_015899) aligner software using default parameters, and count tables were generated using the STAR gencounts feature and full Ensembl GTF annotation file. Differential gene expression analysis was performed using DESeq2 (v1.22.2, RRID:SCR_015687) package in R using default settings.

Heatmaps were generated by applying the regularized log transformation (rlog) to the results data frame produced by the DESeq2 package. To generate figures, the rlog values for filtered genes of interest were loaded into the pheatmap (RRID:SCR_016418) R package and scaled by row. The core network in Figure 2 evaluating the 357 'Adult qMcSC Core' genes was generated using the STRING database (0.4 confidence protein-protein interactions using the experimental, database, and text mining information; v11.0, RRID:SCR_005223). Visualization and optimization of the network layout was performed using Cytoscape (v3.7.1, RRID:SCR_003032) and the plug-in Cyspanning tree (v1.1).[111–113] In brief, unconnected small trees (2-3 nodes) were removed (leaving 267/357 'Adult qMcSC Core' genes) before applying a maximal Kruskal algorithm on the combined evidence scores for edges and a radial layout was used to visualize the resulting branches. Hub proteins and transcription factors were determined by using publicly available data provided by the Enrichr database[114] (RRID:SCR_001575) and AnimalTFDB (RRID:SCR_001624) respectively. SASP genes were identified using the gene set REACTOME_SENESCENCE_ASSOCIATED_SECRETORY_PHENOTYPE_SASP, www.gsea-msigdb.org; and the SASP Atlas, http://www.saspatlas.com/. Enrichment analysis of biological processes was performed using the Molecular Signatures Database (MSigDB v6.2, RRID:SCR_016863) through the Gene Set Enrichment Analysis website platform or the Panther Database (Release 17.0, RRID: RRID:SCR_004869). Visualization of data and generation of the clustered bar graphs were performed using the ggplot2 (RRID:SCR_014601) R-package. This RNA-seq data is available at NCBI GEO, GSE261101.

qRT-PCR analysis

For comparing quiescent and actively proliferating cells, 1 x 10^6 cells were isolated by flow cytometry and 1µg of purified RNA was reverse transcribed into cDNA using the High Capacity cDNA Reverse Transcription Kit (Thermo Fisher Scientific 4368813). For comparing actively proliferating cells after siRNA knockdown, 1µg of purified RNA was reverse transcribed into cDNA using the same kit as above. A standard curve was used to determine the mean quantity value of target transcripts between conditions and across three technical replicates per sample. TaqMan Fast Universal PCR Master Mix (Thermo Fisher Scientific 4444965) and Taqman gene expression assays were used for amplification. Gene expression assays included *Pd-l1* (Cd274, Mm03048248_m1), *Cdk2* (Mm00443947_m1), *Cdk4* (Mm00726334_s1), Cdkn1a (Mm01303209_m1), *Cdkn1b* (Mm00438168_m1), *Cdkn2a* (Mm00494449_m1), *Mki67* (Mm01278617_m1), *Pdcd1* (Mm01285676_m1), *Gapdh* (4352932E), and *Actb* (Mm00607939_s1). Expression was assessed on a QuantStudio3 (Thermo Fisher) using the default fast reaction settings. For comparing actively proliferating cells after siRNA knockdown, gene expression was normalized to the housekeeping gene *Gapdh* or *Actb*. For comparing quiescent and actively proliferating cells, gene expression was normalized by cell number to account for the change in the transcriptome size of cells across cellular states:

$$Relative\ expression = \frac{Mean\ quanity\ value\ of\ sample}{\#\ of\ cells\ in\ 1ug\ cDNA\ reaction}$$

The ratio of cyclin-dependent kinase inhibitors to their respective cyclin-dependent kinases for individual samples across conditions was calculated using the following formula.

$$Ratio = \frac{Average\ Cdkn\ expression}{Average\ Cdk\ expression}$$

Tissue and cell immunolabeling

For immunohistochemistry, the skin was immersed in freshly made 2% methanol-free formaldehyde (Thermo Fisher Scientific 28908) in 1X DPBS (w/o Mg and Ca, Gibco 14190-144) for 2 hours on ice and washed in 1X DPBS at 4°C. Skin samples were cryoprotected by placing them in 10% sucrose (Fisher S5-500) in 1X DPBS for additional 24 hours at 4°C prior to freezing in O.C.T. (Fisher 23-730-571). 8-10 μm thick cryosections of skin were cut using a cryostat (Thermo Fisher Scientific NX50) and stored at -80. Immunolabeling was performed by washing slides in a 1X DPBS and 0.1% Tween 20 (Fisher BP337-500) solution (PBST) for 20 minutes, incubation in primary antibodies overnight at 4°C followed by incubation secondary antibodies for two hours at room temperature.

For immunocytochemistry, cells were grown on 8- or 4-well chamber slides. Cells were washed with 1X DPBS and fixed using 2% methanol-free formaldehyde in 1X DPBS for 30 minutes at room temperature. Immunolabeling was performed by washing slides in a PBST for 20 minutes, incubation in primary antibodies for 30-60 minutes at room temperature followed by incubation in secondary antibodies for 30 minutes at room temperature.

Primary antibodies used for immunolabeling included: anti-PD-L1 (1:500, Thermo Fisher Scientific 14-5982-82, RRID:AB_467781), anti-DCT (1:400, anti-TRP-2, Santa Cruz Biotechnology sc-10451, RRID:AB_793582), and anti-MKI67 (1:100, Abcam ab16667, RRID:AB_302459). Secondary antibodies included AF488 and AF594 (1:2000-1:3000, AlexaFluor, Invitrogen). Following antibody incubation, slides were washed in PBST for 15-20 minutes and coverslips mounted with Fluoromount-G with DAPI (Thermo Fisher Scientific 00-4959-52). Fluorescence microscopy and imaging were performed either on an EVOS FL Cell Imaging System (Thermo Fisher Scientific) or Eclipse 80i microscope (Nikon). Images were processed using Adobe Photoshop.

Hair counts

Hair shaft pigmentation was quantified in (9-week, n=5) and aged (24-month, n=4) C57BL/6J female mice using a binning method developed previously in our lab.[115] Briefly, plucked hairs were classified as high, medium, or low black (depending on the amount of white space within the medullary air pockets), and white (essentially no visible pigment granules). All analyses were performed blind to sample age. A minimum of 200 hairs were counted per adult sample (n=5) and over 1000 hairs per aged sample (n=4).

Quiescence induction in melb-a cells

For assessment of actively proliferating melb-a cells, sub-confluent T-75 filtered flasks (Thermo Fisher Scientific 156499) were split 1:4 into fresh T-75 flasks, incubated in full media, and harvested 24 hours later at roughly 50% confluency. For assessment of quiescent melb-a cells, G_0 was induced using serum deprivation or contact inhibition. Serum deprivation was achieved by first syncing subconfluent cells to the G1 stage of the cell cycle by thoroughly washing the cells in 1X DPBS and incubating them in media without the mitogens SCF and bFGF (RPMI, pen/strep, and 10% hi-FBS). Following mitogen withdrawal, cells were washed with 1X DPBS and incubated in media without mitogens and with low serum (RPMI, pen/strep, and 0.1% hi-FBS) for either 48 (2-day) or 96 (4-day) hours before harvesting. Contact inhibition was achieved by plating cells at 10% confluency (Lo) or 100% confluency (Hi) for 24 hours prior to switching to media with low serum (RPMI, pen/strep, and 0.1% hi-FBS) and with or without mitogens for 72 hours.

PD-L1 blockade and *Pd-l1* knockdown in melb-a cells

For PD-L1 blockade using antibodies, melb-a cells were treated with isotype-matched IgG2b isotype control (LTF-2; BioXCell, RRID:AB_1107780) or PD-L1 antibodies (10F.9G2; rat IgG; BioXCell, RRID:AB_10949073). For the assessment of PD-L1 blockade during entry into quiescence, G0 was induced using serum deprivation as described above. Following mitogen withdrawal and cell washing, cells were incubated in media without mitogens and with low serum (RPMI, pen/strep, and 0.1% hi-FBS) and in the presence of 10ug/mL IgG control or anti-PD-L1 antibody for 48 hours. For assessment during quiescence, serum deprivation was used as described above. Following 48 hours in media without mitogens and with low serum, IgG control or anti-PD-L1 antibody was added to media for 24 hours prior to the assessment of apoptosis by PI staining. For assessment in actively proliferating cells, cells were treated with antibodies in full media for 48 hours prior to assessment.

For *Pd-l1* knockdowns using siRNA, melb-a cells were transfected for 72 hours with dicer-substrate short interfering siRNAs (DsiRNAs TriFECTa Kit, IDT) targeting a scramble sequence (Scrambled Negative Control DsiRNA) or *Pd-l1* (mm.Ri.Cd274.13.1). Transfection of cells was achieved using lipofectamine RNAiMAX (Thermo Fisher Scientific) according to the manufacturer's protocol. Following knockdown, cells were washed and lysed in Trizol for RNA isolation and qRT-PCR analysis or RIPA buffer supplemented with 1X protease inhibitor cocktail (Halt, Thermo Fisher Scientific) for western blot analysis.

All cell counts were performed using a Bio-Rad TC20 automated cell counter. Other assessments were made using flow cytometry.

Flow cytometry of melb-a cells

For the assessment of melb-a cells by flow cytometry or the isolation of melb-a cells by or cell sorting, a single cell suspension was evaluated using a Bio-Rad Se3 cell sorter equipped with 488/561 nm lasers. After cell growth or treatment, cells were trypsinized (Tryple Express, Thermo Fisher Scientific 12604021) and resuspended in freshly prepared FACS wash solution consisting of 1X DPBS, 5% FBS, 25mM HEPES, and 2mM EDTA.

For isolation of specific numbers of cells, a live cell gate was established using forward and side scatter and these cells sorted into individual tubes containing FACS wash solution. For assessment of protein expression, cells in solution were fixed in 2% formaldehyde for 20 minutes at room temperature. Cells evaluated for surface expression (PD-L1) were not permeabilized while those that were evaluated for nuclear expression (MKI67) were permeabilized by treatment with 0.1% Tween for 30 minutes at room temperature. Primary antibodies used for immunolabeling included: anti-PD-L1-PE (1:100, Invitrogen 12-5982-82, RRID:AB_466089) and anti-MKI67 (1:100, Abcam ab16667, RRID:AB_302459). For assessment apoptosis by PI staining, cells were treated with up to 1 μg/ml of PI and analyzed immediately.

For evaluating DNA synthesis by EdU assay, we used the EdU Click-iT assay (Thermo Fisher Scientific C10632) following manufacturer guidelines and carried out at room temperature and protected from light. Briefly, cells were incubated in media supplemented with 10 μM EdU for 2 hours at 37°C and 10% CO2 and washed in 1% BSA in 1X DPBS prior to harvesting. Cells were resuspended in 100 μL of Click-iT fixative for 15 minutes. Cells were washed and resuspended in 100 μL of 1X Click-iT saponin-based permeabilization and wash reagent for an additional 15 minutes before adding 0.5 mL of freshly prepared Click-iT reaction cocktail and incubated for 30 minutes. Cells were washed and resuspended in 500uL 1X Click-iT saponin-based permeabilization and wash reagent and immediately analyzed.

Protein quantification and western blotting

For total protein quantification to compare quiescent and actively proliferating cells, $1x10^6$ melb-a cells were isolated using flow sorting, lysed in RIPA buffer, and total protein was quantified using a standard BCA protocol and Epoch spectrophotometer.

For western blotting of cell lysates, 5 ug of total protein was loaded into wells of a Tris-glycine/SDS/polyacrylamide gel (4% stacking/10% resolving) and electrophoresed at ~80V for 2 hours. Proteins were transferred to a nitrocellulose membrane at 20V for 5-7 minutes using the iBlot 2 dry blotting transfer system (Thermo Fisher Scientific). The blot was blocked in 1X TBS with 3% milk and incubated in primary antibody overnight at 4°C. After washing with 1X TBS with 0.05% Tween (TBST), the blot was incubated in HRP-conjugated secondary antibody for 1 hour at room temperature or overnight at 4°C. After washing with TBST, HRP activity was detected using a chemiluminescent substrate (SuperSignal Pico Plus, Pierce) and imaged. Band densitometry was performed using Image Lab (BioRad). Primary antibodies included anti-PD-L1 (1:200, Thermo Fisher Scientific 14-5982-82, RRID:AB_467781), anti-PCNA (1:1000, Abcam ab29, RRID:AB_303394), and anti-β-ACTIN-HRP (1:1000, Proteintech HRP-60008, RRID:AB_2819183). Secondary antibodies included anti-rat-HRP (1:4000, Proteintech SA00001-15), anti-mouse-HRP (1:10,000, Proteintech, SA00001-1).

QUANTIFICATION AND STATISTICAL ANALYSIS

Unless specified otherwise, data from this study was analyzed using Graphpad Prism (RRID:SCR_002798). Statistical details of each experiment (tests used, value of n, dispersion and precision measures, etc.) are included in the figure legends. A p-value of <0.05 was considered statistically significant. In most cases, sample size was estimated by power calculation based on similar types of data from previous studies. Asterisks included in the figures indicate p-values or adjusted p-values: * < 0.05, ** < 0.01, *** < 0.001, **** < 0.0001.